J Biol Inorg Chem
DOI 10.1007/s00775-015-1283-1

ORIGINAL PAPER

Gold(I) NHC-based homo- and heterobimetallic complexes: synthesis, characterization and evaluation as potential anticancer agents

Benoît Bertrand[1,2] · Anna Citta[3] · Inge L. Franken[2] · Michel Picquet[1] · Alessandra Folda[3] · Valeria Scalcon[4] · Maria Pia Rigobello[3] · Pierre Le Gendre[1] · Angela Casini[2] · Ewen Bodio[1]

Received: 2 April 2015 / Accepted: 12 July 2015
© SBIC 2015

Abstract While *N*-heterocyclic carbenes (NHC) are ubiquitous ligands in catalysis for organic or industrial syntheses, their potential to form transition metal complexes for medicinal applications has still to be exploited. Within this frame, we synthesized new homo- and heterobimetallic complexes based on the Au(I)–NHC scaffold. The compounds were synthesized via a microwave-assisted method developed in our laboratories using Au(I)–NHC complexes carrying a pentafluorophenol ester moiety and another Au(I) phosphane complex or a bipyridine ligand bearing a pendant amine function. Thus, we developed two different methods to prepare homo- and heterobimetallic complexes (Au(I)/Au(I) or Au(I)/Cu(II), Au(I)/Ru(II), respectively). All the compounds were fully characterized by several spectroscopic techniques including far infrared, and were tested for their antiproliferative effects in a series of human cancer cells. They showed moderate anticancer properties. Their toxic effects were also studied ex vivo using the precision-cut tissue slices (PCTS) technique and initial results concerning their reactivity with the seleno-enzyme thioredoxin reductase were obtained.

Keywords *N*-heterocyclic carbene · Bimetallic complex · Gold complex · Anticancer drug · Thioredoxin reductase

Electronic supplementary material The online version of this article (doi:10.1007/s00775-015-1283-1) contains supplementary material, which is available to authorized users.

✉ Angela Casini
a.casini@rug.nl

✉ Ewen Bodio
Ewen.Bodio@u-bourgogne.fr

1 Institut de Chimie Moléculaire, UMR 6302 CNRS Université de Bourgogne Franche Comté, 9 Avenue A. Savary, 21078 Dijon, France

2 Department of Pharmacokinetics, Toxicology and Targeting, Research Institute of Pharmacy, University of Groningen, Antonius Deusinglaan 1, Groningen 9713 AV, The Netherlands

3 Department of Biomedical Sciences, University of Padova, via Ugo Bassi 58/b, Padua, Italy

4 Institute of Neuroscience, C.N.R., viale G. Colombo 3, Padua, Italy

Introduction

Metal-based drugs represent one of the most used and studied classes of anticancer chemotherapeutic agents. For example, the platinum-based drugs cisplatin, carboplatin and oxaliplatin, are present in a plethora of chemotherapeutic treatments [1, 2]. However, despite their clinical success, Pt(II) drugs present major drawbacks, such as a limited spectrum of action, development of drug resistance, and severe side effects that narrow their range of applicability. During the last few decades numerous transition metals were investigated to circumvent these issues. Among them, promising results were obtained for ruthenium, copper, gold and titanium coordination and organometallic compounds [3–8]. For example, gold(I) complexes have appeared in the last decades as very potent cytotoxic agents, [9–13] the most well-known example being [(2,3,4,6-tetra-*O*-acetyl-1-(thio-κS)-β-D-glucopyranosato)(triethyl-phosphane) gold(I)] (auranofin), which is used clinically as an anti-arthritis agent. Today this compound is in clinical trials for the treatment of several types of cancer (Fig. 1) [14–16].

Structure–activity relationships studies on several auranofin analogues showed the importance of the

Published online: 23 July 2015

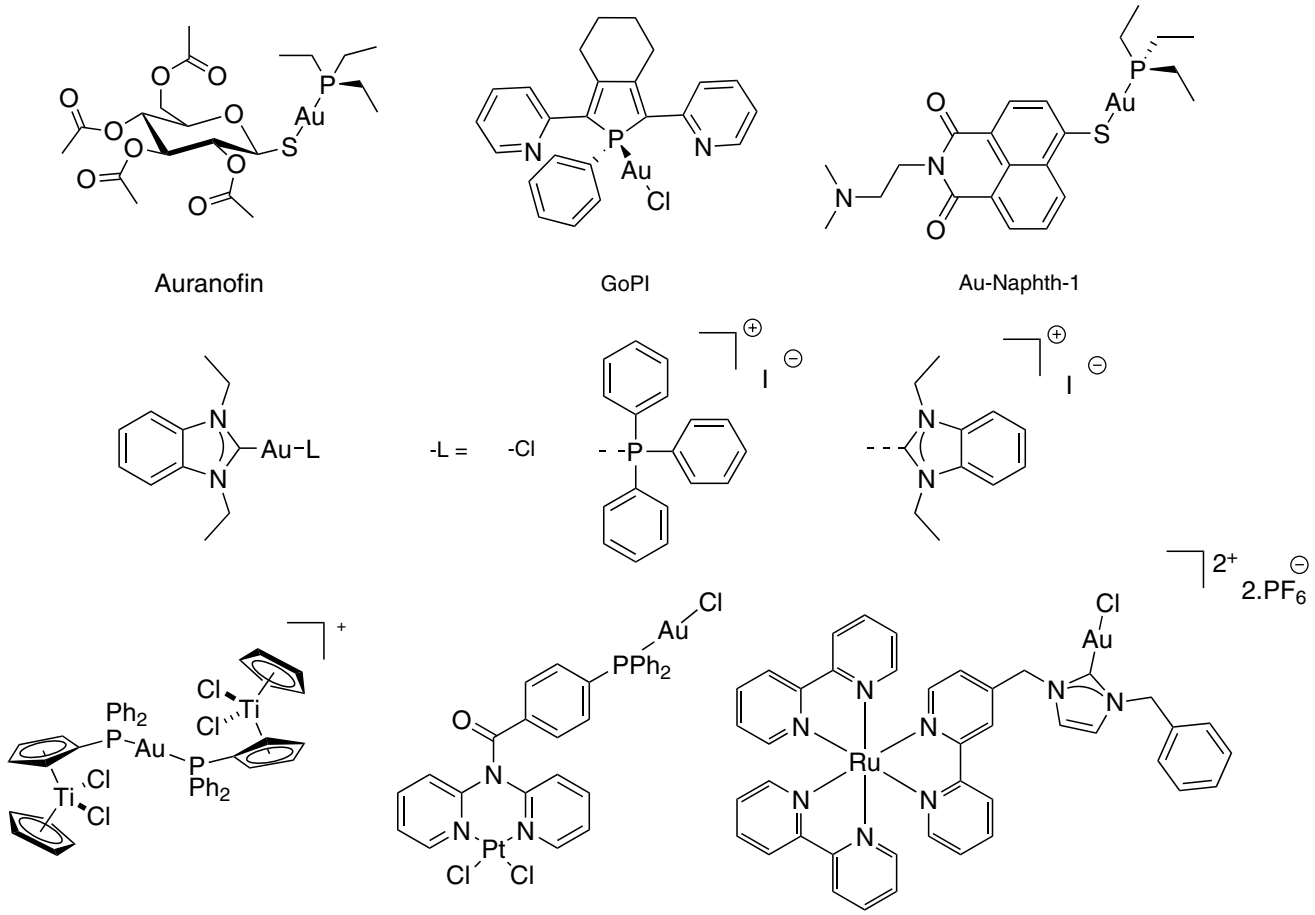

Fig. 1 Examples of phosphane gold(I) complexes, NHC gold(I) complexes, and heteropolymetallic complexes

phosphane for toxicity [17]. Other studies on complexes of the general formula R_3P–Au(I)–Cl (where R = alkyl or aryl) showed a positive correlation between the size of the substituents on the phosphorous atom and cellular uptake and toxicity [18]. The development of gold(I)–phosphole chloride (GoPI) (Fig. 1) and its thiosugar analogue (GoPI-sugar) led to cytotoxic activities in the low micromolar range against glioblastoma or breast cancer cells in vitro [19, 20]. Ott et al. combined Et_3P–Au(I) with an anticancer agent that acts through DNA intercalation [21, 22]. The resulting Au–Naphth-1 compound (Fig. 1) was revealed to be as toxic as Et_3P–Au–Cl in vitro. Gimeno et al. reported the synthesis of a phosphane Au(I) complex one order of magnitude more effective than auranofin against a cervical cancer cell line [23].

The successful application of phosphanes as ligands for the synthesis of gold(I) potential chemotherapeutic agents led researchers to study other "L" type ligands such as *N*-heterocyclic carbenes (NHC) carbenes. For example, Berners-Price et al. have synthesized a variety of organometallic cationic mononuclear gold(I) biscarbene complexes, tuning the lipophilic character of the complexes by varying the wingtip groups [24–26]. These gold organometallic molecules display strong antimitochondrial effects.

In addition to varying lipophilicity, the presence of a second ancillary ligand coordinated to gold is a critical factor to regulate the biological properties of the gold complexes. Indeed, Rubbiani et al. synthesized three NHC gold(I) complexes of the 1,3-benzimidazol-2-ylidene type (Fig. 1) with different ligands (Cl, NHC, and PPh_3, respectively) [27]. As the chlorido and phosphane derivatives are more prone to ligand substitution reactions, they are stronger inhibitors of the seleno-enzyme thioredoxin reductase (TrxR) than the cationic biscarbene.

Concerning possible mechanisms of action, as previously mentioned, a large number of metal complexes and organometallic compounds target TrxR [28–31]. Two major systems play a critical role in the control of cellular thiol redox regulation, namely thioredoxin (Trx) and glutathione (GSH).

The first system is formed by TrxR, which is reduced by NADPH and in turn maintains Trx in the reduced form [32, 33]. In addition to other functions, Trx acts as an electron donor for the family of peroxiredoxins that catalyse the

reduction of H_2O_2 to water [34]. TrxRs are dimeric proteins endowed with a N-terminal redox centre with a dithiol motif and a C-terminal active site with a Cys-Sec motif. The Sec residue has a low pKa, resulting in enhanced nucleophilic properties [35]. Thus, inhibition of TrxR by metal compounds has been shown to occur at the nanomolar to low micromolar level and this often correlates with their antiproliferative effects in vitro. The mechanism of inhibition essentially involves metal binding to the Sec residue at the TrxR *C*-terminus [36]. Two isoforms, a cytosolic (TrxR1) and a mitochondrial (TrxR2), are found in cells [37, 38]. TrxR is considered a relevant target for the development of anticancer agents in particular because of its overexpression in cancer cells [39, 40]. In recent papers, NHC gold(I) compounds were shown to target both TrxR isoforms preferentially in tumour cell lines rather than in normal cells [41]. TrxR inhibition determines a shift to the oxidized forms of Trx and Prx III, allowing a large increase in reactive oxygen species (ROS) [42].

The second intracellular redox system is based on GSH, kept in a reduced state by glutathione reductase (GR), which is itself reduced by NADPH. Glutathione peroxidase (GPx), another selenoenzyme able to detoxify H_2O_2 to water, uses glutathione as a reducing substrate and, with peroxiredoxins, contributes to the maintenance of the cell redox balance [43].

Previously reported analyses, including our own, demonstrated that heterobimetallic complexes were worth studying (Fig. 1) [44–48]. Indeed, multinuclearity often increases cytotoxicity and/or selectivity and the phenomenon of resistance is overcome because of the combined properties, and sometimes the mechanism of action of the two metal moieties. A recent study by Hemmert and coworkers reported on the synthesis and biological evaluation of bimetallic NHC–Au/Ru(bipy)$_3$ complexes [48]. However, the scope of bimetallic complexes that are accessible by their synthesis strategy is quite limited.

In the present work, we chose first to synthesize new gold(I) homobimetallic complexes containing one or two thioglucose tetraacetate moieties. Then we grafted the gold–NHC moiety to a bipyridine to have easy access to gold(I)–ruthenium(II) and gold(I)–copper(II) complexes. Such combinations may induce some synergy phenomenon because their mechanisms of action are believed to be different: Au(I)–NHC are reported to target TrxR, while different studies on "N_2"–Ru(II)–arene or polypyridyl–Cu(II)–Cl_x complexes seem to indicate that they target DNA. We used a procedure inspired by Metzler-Nolte et al. to obtain easily derivatizable gold–NHC complexes [49, 50]. This microwave-assisted strategy recently enabled us to synthesize a homobimetallic gold complex displaying promising antiproliferative properties against a cancer cell line (A2780, an ovarian carcinoma cell line) (Scheme 1) [50].

Assessment of the antiproliferative properties of the new compounds in human ovarian cancer cells (A2780, SKOV-3) and human lung cancer cells (A549) is also reported demonstrating the suitability of these scaffolds for biological applications. The toxicity of the most promising compounds on healthy tissues has been studied using an ex vivo model, namely precision-cut tissue slices (PCTS) [51]. PCTS are viable tissue explants cultured ex vivo, where cell-types are in their natural environment, providing toxicity results that are expected to be more relevant than those obtained in cell cultures. The technique is an FDA-approved model for studies of drug toxicity and metabolism. It was previously used for the assessment of toxicity of metal-based compounds like cisplatin (kidney), [52] experimental gold compounds (liver, kidney and colon) [53] and aminoferrocene-containing pro-drugs (liver) [54]. In the present study, we investigated the effects of **2**, **3**, **4** Au(I) homobimetallic compounds, mononuclear **6** Cu(II) and **7** Ru(II) complexes, and Au(I) mononuclear **5** and heterobimetallic **8** compounds, on the activity of the isolated TrxR seleno-enzyme, and on the homologous enzyme glutathione reductase.

Results

Synthesis and characterization

Replacing the chlorido ligand that is coordinated on the gold centre by an acetylated thioglucose moiety, as in auranofin, often increases the cytotoxicity of the resulting metal complex [47, 55, 56]. Thus, we first attempted to coordinate the thiosugar derivative on the gold centre of compound **1**. However, this reaction turned out not to be regioselective. Therefore, instead we introduced the sugar derivative on the Au(I)–P side. For this purpose, [Au($H_2N(CH_2)_2PPh_2$)Cl] precursor **A** was reacted with one equivalent of thio-β-D-glucose tetraacetate following a modified procedure found in the literature, [57] as depicted in Scheme 2. The formation of compound **B** was confirmed, among all, by [58] P{^{1}H} NMR analysis, where the phosphorous atom gave rise to a broad singlet shifted 4 ppm downfield from the corresponding signal in **A**. This is in agreement with the substitution of the chlorido ligand by a thiolato one [47]. Moreover, in the far-infrared (FIR) spectrum, the ν_{Au-Cl} vibration band was replaced by a broader and less intense ν_{Au-S} band at 372 cm^{-1} [58]. The microwave-assisted coupling reaction of compounds **1** with **B** led to the formation of the homobimetallic complex **3** with two differently substituted gold centres in good yield (Scheme 1).

It is worth noting that no additional base was used to prevent any degradation of the carbene. The ^{19}F{^{1}H} NMR

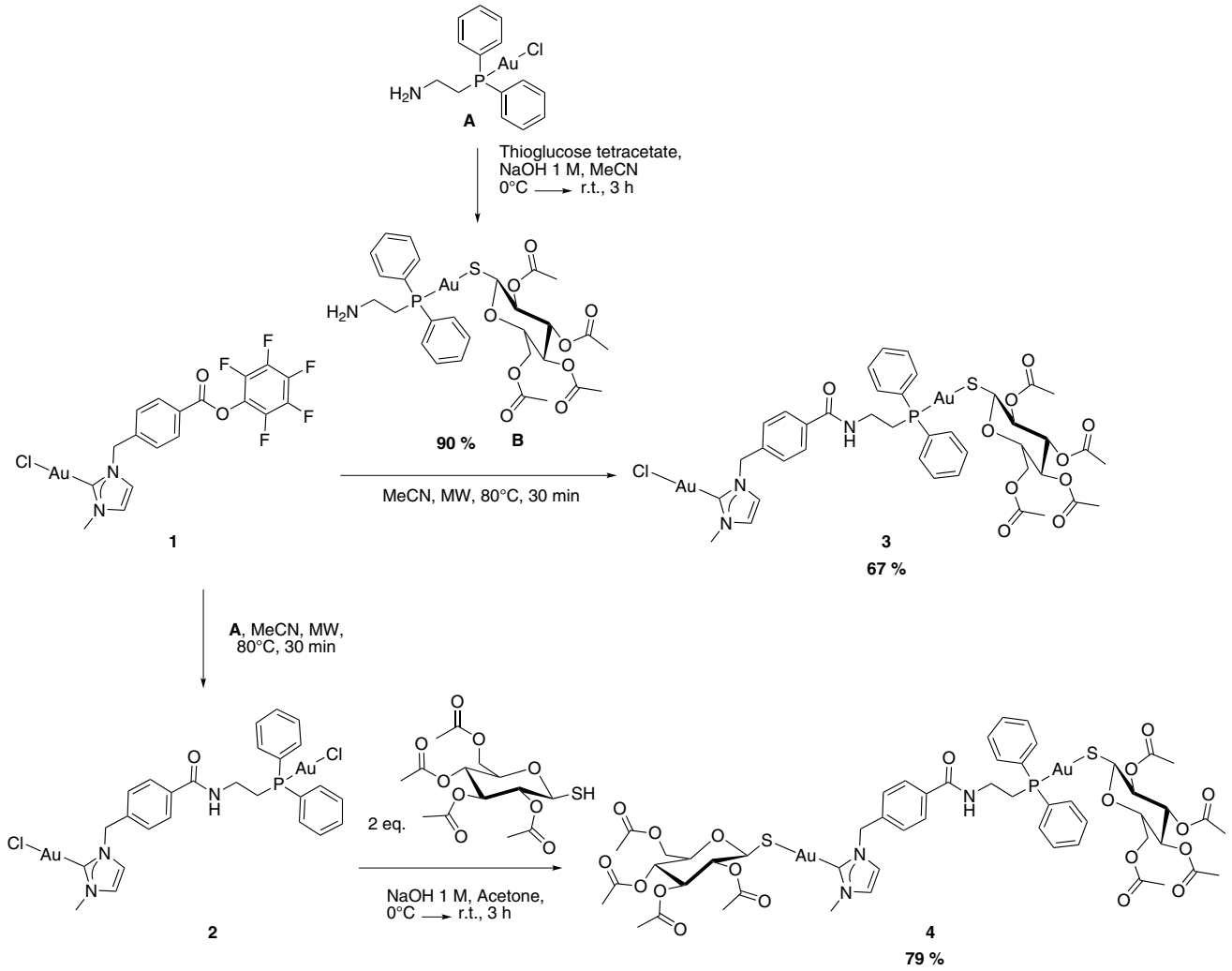

Scheme 1 Synthesis of gold(I) homobimetallic complexes **3** and **4**

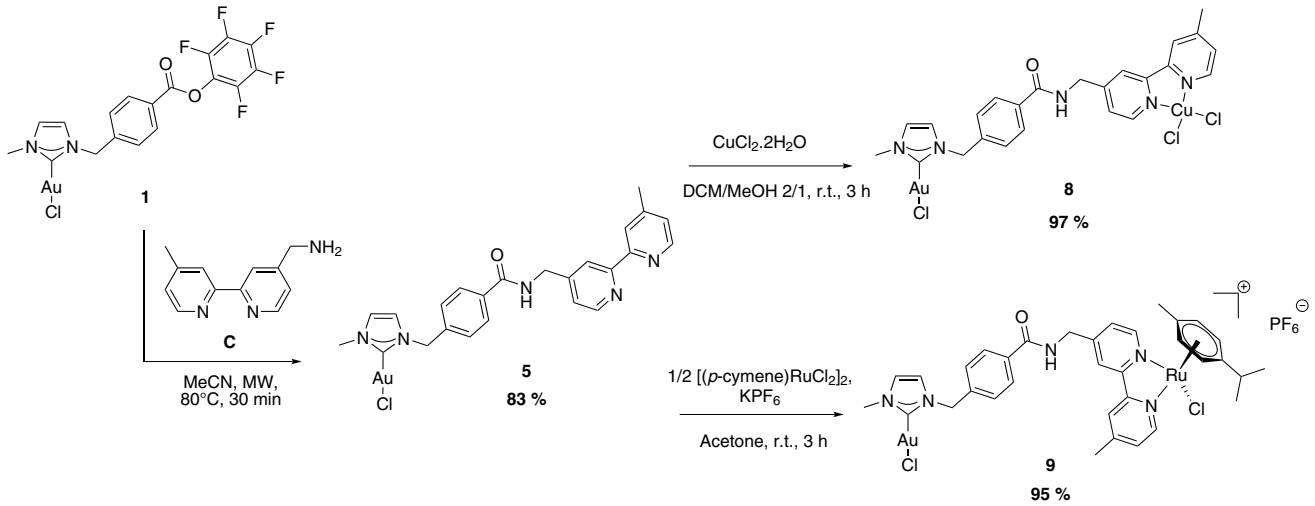

Scheme 2 Synthesis of heterobimetallic complexes **8** and **9**

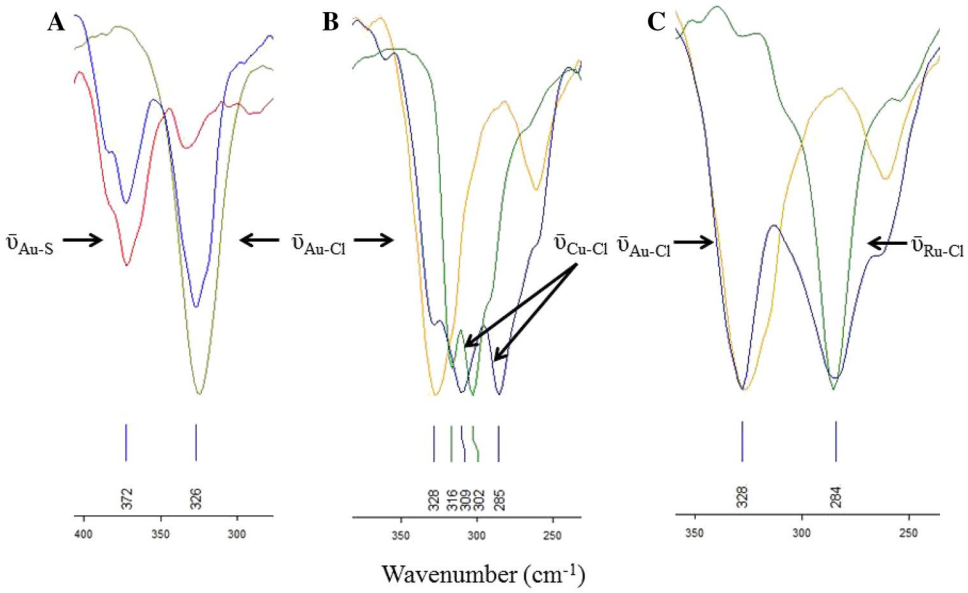

Fig. 2 Far-infrared spectra in the $\nu_{M\text{-}X}$ area. **a** Spectra of complexes **2** (*green*), **3** (*blue*) and **4** (*red*). **b** Spectra of complexes **5** (*orange*), **6** (*green*) and **8** (*blue*). **c** Spectra of complexes **5** (*orange*), **7** (*green*) and **9** (*blue*)

spectrum of compound **3** showed the disappearance of the pentafluorophenol signals. Moreover, the ^{1}H NMR spectrum displayed a downshift of all signals of the NHC moiety compared to the spectrum of the starting complex **1**, associated with a downfield shift of the N–CH_2 signal in the ethylenic linker from 3.06 to 3.10 ppm. This phenomenon was associated with the appearance of a broad singlet at 6.2 ppm corresponding to the N*H* proton. Additionally, in the ^{13}C{^{1}H} NMR spectrum, the C(O) signal of was shifted from 161 ppm in the activated ester to 167 ppm in the amide, confirming the reaction of the perfluorinated ester moiety. The comparison of the IR spectra showed a shift of the carbonyl group vibration band from 1715 to 1640 cm^{-1}. Complex **3** was also characterized by high-resolution mass spectrometry and elemental analysis and all these data were in agreement with the formation of an amide linkage. Although no diastereotopic splitting due to the presence of the optically active sugar was observed in the case of compound **B**, both CH_2–P and CH_2–N appeared as AB systems in the ^{1}H NMR spectrum of molecule **3**. The ^{31}P{^{1}H} NMR spectrum of the crude product showed the presence of 5 % of redistribution product (complex in which the thiolato ligand was shifted from the Au–P centre to the Au–NHC one) indicated by a narrower singlet at 24 ppm corresponding to a P–Au–Cl moiety. However, by precipitation from a solution of dichloromethane using a small amount of diethyl ether, it was possible to obtain pure complex **3**. The FIR spectrum of compound **3** presented two vibration bands corresponding to the two different Au–X bonds. The Au–Cl bond gave rise to a narrow band at 325 cm^{-1} while the Au–S bond gave rise to a broader band at 372 cm^{-1} (Fig. 2a).

To complete the series of homobimetallic Au(I)/Au(I) complexes, complex **2** was reacted with two equivalents of thio-β-D-glucose tetraacetate in acetone to obtain in good yield the homobimetallic complex **4** with two thiosugar moieties (Scheme 1). The compound **4** FIR spectrum presented the typical $\nu_{Au\text{–}S}$ vibration band at 372 cm^{-1} (Fig. 2a). As we previously found in the case of compound **2**, both Au–S bonds gave rise to a unique vibration band confirming the equivalence of the thiolato ligands we observed in ^{1}H NMR.

We next focused our study on the development of a series of late/late heterobimetallic complexes. The combinations of the Au(I)–NHC moiety with platinum, ruthenium or copper fragments were investigated for their potential to create synergistic effects and to enhance compounds' cytotoxicity. Thus, we decided to introduce a bipyridine moiety as second ligand in the Au(I) NHC scaffold. This choice was based on the versatility of bipyridine which enables the complexation of a broad spectrum of metal ions (e.g. ruthenium, iron, copper, platinum and rhenium) [59–61]. Complex **1** was reacted with (4′-methyl-[2,2′-bipyridin]4-yl) methamine **C** following the previously described procedure. The desired gold(I)–NHC complex bearing a free bipyridine ligand **5** was obtained in a very good yield (Scheme 2).

4,4′-dimethyl-2,2′-bipyridine **D** was used as a model before performing the reaction with **5** (Scheme 3). One equivalent of **D** was reacted with one equivalent of $CuCl_2.2H_2O$ at room temperature for 3 h. The synthesis of **6** had been previously described by Sadler et al. and performed in methanol [62]. However, due to the low solubility of **5** in methanol, we optimized the metallation conditions using a mixture of dichloromethane and methanol or acetone as solvent. The expected copper and ruthenium complexes **6** and **7** were obtained in 97 and 98 %

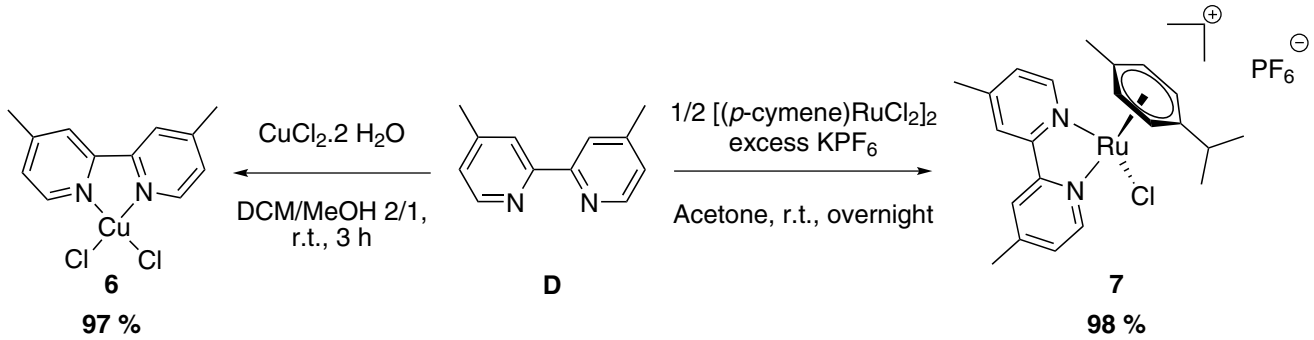

Scheme 3 Synthesis of the copper(II) and ruthenium(II) based model complexes **6** and **7**

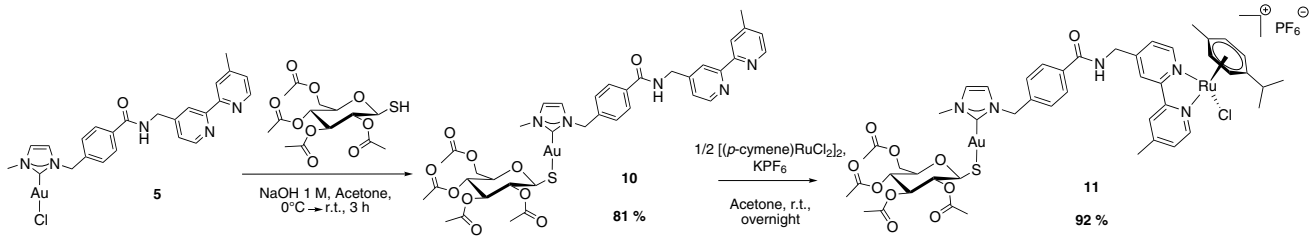

Scheme 4 Synthesis of complexes **10** and **11**

yield, respectively (Scheme 3). Due to the paramagnetic copper(II) cation, **6** was not studied by NMR, but its composition was assessed by elemental analysis and high-resolution mass spectrometry. The ^{1}H NMR spectrum of **7** corresponds to the data provided by Sadler et al. FIR spectra of both compounds **6** and **7** have been recorded and these showed vibration bands at 316 and 303 cm^{-1} attributed to ν_{Cu-Cl} and at 286 cm^{-1} attributed to ν_{Ru-Cl} that confirmed the formation of the model complexes (Fig. 2b, c) [63, 64].

These encouraging results prompted us to perform the same reactions on **5.** The two heterobimetallic complexes Au(I)/Cu(II) **8** and Au(I)/Ru(II) **9** were obtained in yield 97 and 95 %, respectively (Scheme 2). The structure of **8** was assessed by elemental analysis and high-resolution mass spectrometry. The formation of **9** was demonstrated by ^{1}H NMR, with signals corresponding to the protons in positions 6 and 6′ shifted from 8.50 ppm in **5** to 9.39 and 9.46 ppm upon the chelation of ruthenium.

Moreover, the diastereotopic splitting of the signals of the two methyl groups of the isopropyl residue in complex **9** confirmed the coordination of the arene–Ru moiety by an unsymmetrically substituted bipyridine. The FIR spectra of **8** showed the three metal–chloride vibration bands ν_{Au-Cl} at 328 cm^{-1} and two ν_{Cu-Cl} bands at 310 and 286 cm^{-1}, identically to the monometallic precursors **1** and **6** (Fig. 2b). Similarly, the FIR spectra of complex **9** displayed two metal–chloride vibration bands ν_{Au-Cl} and ν_{Ru-Cl} at 328 and 284 cm^{-1}, respectively, corresponding to both monometallic analogues **1** and **7** as seen in the case of the Au(I)/Cu(II) bimetallic complex **8** (Fig. 2c).

We decided to replace the chlorido ligand on the gold atom by thio-β-D-glucose tertraacetate. Thus, one equivalent of the thioglucose derivative was reacted with **5** to afford compound **10** (Scheme 4). Beyond the expected 1/1 ratio between the thiosugar derivative and the NHC-free bipyridine moiety, the ^{1}H NMR spectrum of **10** showed a splitting of the singlet corresponding to the protons of the N–CH_2 bridge to an AB-type system. Thus, we assessed the coupling of the optically active thiosugar to the gold centre. Moreover, the coordination through the sulphur atom was confirmed by FIR spectroscopy.

Complex **10** was then reacted with $CuCl_2{\cdot}2H_2O$ and half an equivalent of [(*p*-cymene)$RuCl_2$]$_2$ following the procedures we previously applied to the syntheses of the heterobimetallic complexes **8** and **9** (Scheme 4). Although the heterobimetallic complex Au(I)/Ru(II) **11** was obtained in a yield comparable to those of **7** and **9**, the reaction between **10** and $CuCl_2{\cdot}2H_2O$ failed (see Electronic Supplementary Material for details). The ^{1}H NMR spectrum of the bimetallic complex **11** was difficult to interpret. Indeed complex **11** is a 1/1 ratio mixture of two diastereoisomers emerging from the association of the optically pure thiosugar derivative with the metal-centred chiral arene–ruthenium moiety.

Thus, all signals were doubled because of the two diastereoisomers, all CH_2 signals appearing additionally split into AB systems. However, we noticed the same downfield

shift of almost 1 ppm for the closest protons to the nitrogen atoms from 8.5 and 8.6 to 9.4 and 9.5 ppm, as seen in the case of complex **9**. The same profile was seen in the $^{13}C\{^{1}H\}$ NMR spectrum where all signals were again doubled. The FIR spectrum of **11** showed a broad band at 375 cm^{-1} corresponding to the Au–S bond and another one at 287 cm^{-1} in agreement with the corresponding bands in the cases of complexes **7** and **10** (see Fig. S1 in Electronic Supplementary Material). These data, in association with the elemental analysis and the high-resolution mass spectrum, enabled us to confirm the structure of the expected heterobimetallic complex **11.**

Antiproliferative activity in vitro

The novel compounds were screened for their antiproliferative properties in human ovarian cancer cell lines sensitive to cisplatin (A2780), resistant to cisplatin (SKOV-3) and human lung cancer cells (A549) using the classical MTT assay (see Experimental section for details). Dose-dependent inhibition of cell growth was observed in all cell lines with IC_{50} values ranging from approximately 2 to above 100 μM after 72 h incubation as depicted in Table 1.

The antiproliferative properties of compound **2** have already been demonstrated in the human ovarian cancer cell line A2780 showing activity comparable to cisplatin ($IC_{50} = 2.2 \pm 0.4$ μM and 1.9 ± 0.4 μM respectively) [50]. In general, all the new compounds reported were much more effective in the A2780 cell line than in other ovarian cancer cells (SKOV3) or A549 lung cancer cells. Previous studies reported the increasing toxicity and increased uptake of gold-based compounds due to the presence of the thio-*β*-D-glucose tetraacetate moiety [47, 55, 56]. However, in the case of the dinuclear Au(I) complexes **3**–**4**, this strategy did not improve the antiproliferative properties of the homobimetallic scaffold compared to the precursor **2** (Table 1) on any cell lines.

Concerning the heteronuclear complexes, it was observed that by adding the Cu(II) cation to the gold–bipyridine scaffold as in complex **8**, the IC_{50} values decreased consistently in the case of all cell lines in comparison to the mononuclear Au(I) precursor **5**. This effect may be attributed to the presence of the Cu(II) ions having major antiproliferative properties on their own, as could be seen in the case of the (4,4′-dimethyl-2,2′-bipyridine)copper(II) dichloride complex **6**.

In contrast, by adding the ruthenium moiety to the gold-based compound, a decrease of toxicity of the heterobimetallic compound **9** was noticed when compared to the gold precursor **5**. Compound **9** behaved similarly to the non-toxic ruthenium monometallic precursor **7** (IC_{50} >100 μM in all cell lines). These results suggested that the choice of the second metal on the Au(I) NHC scaffold is determinant to fine-tune the biological effects of the resulting compound. Finally, in the case of compound **11**, which bears both the thio-*β*-D-glucose tetraacetate ligands bound to the Au(I) and Ru(II)–arene moieties, we noted an increase in the selectivity of the compound for the A2780 cell type with respect to the chlorido precursor **5**.

Table 1 Inhibition of cell viability (IC_{50} values) in human ovarian carcinoma cell lines (A2780, SKOV-3) and human lung cancer cells (A549), after 72 h incubation with compounds **1**–**11** or cisplatin

IC_{50} (μM)			
Compound	A2780	SKOV-3	A549
Cisplatin	2.3 ± 0.3	14.6 ± 2.0	11 ± 0.4
1	53.0 ± 2.4[a]	n. d.	n. d.
2	2.2 ± 0.4[a]	67 ± 10	37.0 ± 3.7
3	5.8 ± 1.7	55 ± 10	38.6 ± 1.4
4	5.0 ± 1.3	65.9 ± 6.6	72.6 ± 4.7
5	21.8 ± 3.6	75 ± 19	58.8 ± 6.5
6	2.3 ± 0.6	9.7 ± 0.5	6.1 ± 0.9
7	>100	>100	>100
8	10.3 ± 0.5	21.1 ± 4.5	23.6 ± 2.7
9	63.4 ± 2.4	>100	>100
10	16.1 ± 2.7	36.7 ± 4.9	26.8 ± 1.5
11	16.8 ± 3.1	>100	>100

[a] Data from ref. [50]

Ex vivo toxicity studies

Based on the in vitro study we selected the dinuclear Au(I) compound **2**, and the heteronuclear Au(I)–Cu(II) complex **8**, both of which were among the most active of the new series of molecules. These compounds were evaluated for their toxicity against healthy liver tissue in an ex vivo model using precision-cut liver slices (PCLS) [51]. We also included the compounds **5** (Au) and **6** (Cu) in this assay to investigate the contribution of the single metal entities to possible toxic effects. Thus, rat liver tissues were incubated for 24 h with concentrations of compounds ranging from 1 to 30 μM. The viability of the liver slices was assessed by the quantification of their ATP content as described in the Experimental section. The results obtained are depicted in Fig. 3, and they showed a concentration-dependent toxicity for all the compounds on PCLS.

Overall, the results showed a general toxicity of all compounds tested in the liver tissues. In particular, liver slices presented a significant decrease of viability upon incubation with the homobimetallic compound **2** starting from a concentration of 1 μM (Fig. 3). The monometallic compounds **5** and **6** appear to be slightly less toxic. For example, the gold compound **5** showed significant toxic effects on the slices starting from a concentration of 5 μM (Fig. 3).

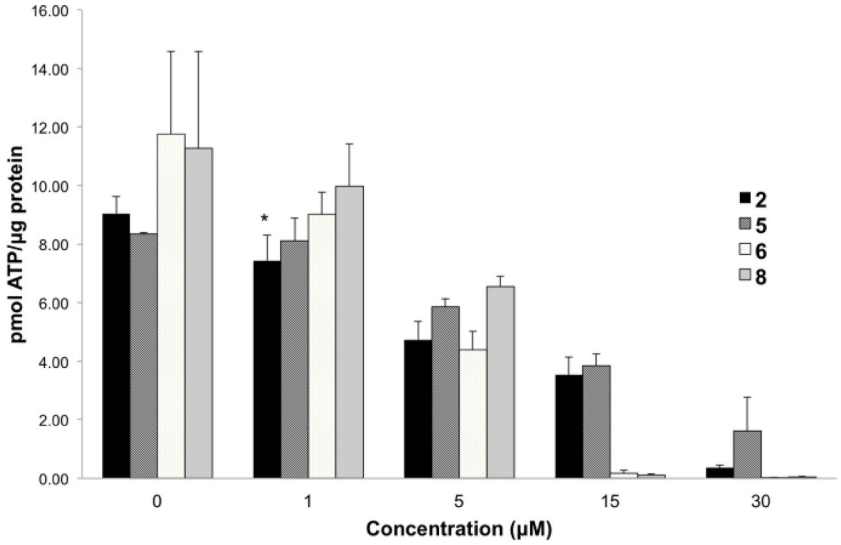

Fig. 3 Viability of rat liver PCLS after treatment with compounds **2**, **5**, **6**, or **8** for 24 h. Values depicted are the mean of two or three independent experiments. The significance of the results was analysed by ANOVA with respect to control samples. *p value <0.05

Table 2 Inhibition of cytosolic (TrxR1), mitochondrial (TrxR2) thioredoxin reductase and glutathione reductase (GR) by compounds **2**, **3**, **4**, **5**, **6**, **7**, and **8**

IC_{50} (nM)			
Compound	TrxR1	TrxR2	GR
2	6.8 ± 0.5	19.7 ± 2.5	110 ± 20
3	4.6 ± 0.2	19.4 ± 2.3	480 ± 25
4	1.7 ± 0.3	18.9 ± 1.5	>10,000
5	8.2 ± 0.1	22.0 ± 8.5	850 ± 26
6	>20,000	>10,000	>40,000
7	>20,000	>10,000	>40,000
8	20.1 ± 0.5	220 ± 12.3	2000 ± 104

The Au(I)/Cu(II) heterometallic complex **8** was also found to be significantly toxic against liver tissues starting from a concentration of 5 µM. At this concentration, viability of the slices was reduced by about 40 %.

Enzyme inhibition studies

Compounds were tested for their properties as inhibitors of cytosolic and mitochondrial TrxR and GR. IC_{50} values for enzyme inhibition are reported in Table 2. As shown in Fig. S2 of the Electronic Supplementary Material, Au(I) homobimetallic compounds **2**, **3**, and **4** at nanomolar levels are powerful inhibitors of TrxR1. The effect increases in the presence of two thio-β-D-glucose tetraacetate ligands with **4** showing an IC_{50} of 1.7 nM. Compounds **5** and **8** in the nanomolar range inhibit TrxR1, but are less effective than homo Au(I) bimetallic compounds. Up to the micromolar range, copper and ruthenium monometallic compounds **6** and **7**, do not show any effect on TrxR1. The activity of TrxR2, the mitochondrial isoform, was also strongly decreased in the presence of compounds **2**, **3**, **4**, **5**, and **8** (Table 2 and Fig. S2D and S2E), but only at higher concentrations. No effects were observed in the presence of compounds **6** or **7**, which may support the idea of other targets for Cu and Ru complexes. Interestingly, in contrast to what we observed for **7**, other Ru–arene complexes of the (p-cymene)(NHC)$RuCl_2$ type have been reported to be good inhibitors of TrxR [65]. Moreover, the cathepsins cysteine proteases have been shown to be inhibited by other families of Ru–arene complexes, [31] while protein tyrosine phosphatases are good targets for Cu compounds [66].

Concerning the Au/Cu heterobimetallic compound **8**, a decrease in the inhibition on TrxRs was seen when compared to the gold precursor **5**, but **8** showed an enhancement of activity compared to the copper monometallic compound **6**. GR was scarcely affected by some of these compounds (**2**, **3** and **4**), where inhibition was observed only at relatively high concentrations (in the range of 0.1–2 µM).

Discussion

We have reported here the synthesis in good yields of seven unsymmetrical bimetallic complexes based on the Au(I)–NHC moiety. We followed two different strategies: the first one, consisting of the grafting of differently substituted Au(I) complexes onto the gold centre, is a quick and selective synthesis of homobimetallic complexes while the second, involving a bipyridine fragment, requires more synthetic steps but allows a broader scope of heterobimetallic complexes to be realized. The structures of the newly synthesized complexes were assessed using different techniques including ^{1}H, $^{13}C\{^{1}H\}$ and $^{31}P\{^{1}H\}$ NMR spectroscopy, IR and FIR spectroscopy, high-resolution mass spectrometry and elemental analysis.

The results of cytotoxicity studies on the different classes of bimetallic complexes showed interesting biological properties. The addition of thiosugar moieties tended to increase the cytotoxicity of the Au–bipyridine monometallic scaffold but not of the Au/Au homobimetallic scaffold. Moreover, the Au/Cu complex **8** appeared to be the most cytotoxic among the newly synthesized bimetallic compounds, being as active as cisplatin against the SKOV-3 cell line. These results suggest that the choice of the second metal on the Au(I) NHC scaffold is determinant to fine-tune the biological effects of the resulting compound. Regarding the Au/Ru heterobimetallic complexes, the Au compound with a chlorido ligand **9** appeared to be inactive on all cell lines tested, whereas the analogue bearing a thiolato-β-D-glucose tetraacetate **11** appeared to be selectively cytotoxic in A2780 cells. The gold(I) mono- and polynuclear compounds were also shown to be potent TrxR inhibitors in the nM range in vitro. In the case of the mononuclear Cu(II) complex **6** the fact that there is no correlation between its marked cytotoxic activity and the poor TrxR inhibition is not unexpected, since other mechanisms are known to be responsible for Cu(II) complex cytotoxic effects, including the inhibition of protein tyrosine phosphatases [66] and the influence on cell redox pathways, [67, 68] as well as DNA damage [69].

Finally, the toxicity of selected compounds on healthy liver tissues was investigated ex vivo using precision-cut rat liver slices. The compounds appeared to be toxic against the liver tissues at concentrations in the low micromolar range. Thus, additional efforts should be devoted to the design of more selective anticancer compounds.

Conclusions

A novel series of homo- and heterobimetallic gold complexes has been described and characterized for their biological effects. Although further studies should be undertaken to investigate the mechanisms of action of this new series of compounds, in vitro antiproliferative assays have revealed promising cytotoxic properties of the compounds in cancer cells and have allowed initial structure–activity relationships to be established. Overall, we are confident that these results will allow new possibilities of fine-tuning of the chemico-physical properties of organometallic Au(I)–NHC scaffolds for biological applications.

Materials and methods

General remarks

All reactions were carried out under an atmosphere of purified argon using Schlenk techniques. Solvents were dried and distilled under argon before use. The precursors [AuCl(tht)], [70] [AuCl($H_2N(CH_2)_2PPh_2$)] **A**, [71] (4′-methyl-[2,2′-bipyridin]4-yl)methamine **C**, [72] and compound **2** [50] have been synthesized according to literature procedures. All other reagents were commercially available and used as received. All the analyses were performed at the "Plateforme d'Analyses Chimiques et de Synthèse Moléculaire de l'Université de Bourgogne". The identity and purity (≥95 %) of the complexes were unambiguously established using high-resolution mass spectrometry and NMR (except for paramagnetic Cu compounds). Exact mass of the synthesized complexes was obtained on a Thermo LTQ Orbitrap XL. ^{1}H- (300.13, 500.13 or 600.23 MHz), ^{13}C- (125.77 or 150.90 MHz), ^{31}P- (202.45 or 242.96 MHz) and ^{19}F- (282.38 MHz) NMR spectra were recorded on Bruker 300 Avance III, 500 Avance III or 600 Avance II spectrometers. Chemical shifts are quoted in ppm (δ) relative to TMS (^{1}H and ^{13}C) and $CFCl_3$ (^{19}F), using the residual protonated solvent (^{1}H) or the deuterated solvent (^{13}C) as internal standards. Alternatively, 85 % H_3PO_4 (^{31}P) and $CFCl_3$ (^{19}F) were used as an external standard. Infrared spectra and far-infrared spectra were recorded on a Bruker Vector 22 FT-IR spectrophotometer (Golden Gate ATR) and on a Bruker Vertex 70v (Platinum ATR), respectively. Microwave reactions were carried on in an Anton Paar Monowave 300 apparatus.

Synthesis

2-Aminoethyldiphenylphosphane gold(I) thiolato-β-D-glucose tetraacetate (B)

A Schlenk tube was charged under argon with thio-β-D-glucose tetraacetate (1 eq., 55 mg, 0.15 mmol) dissolved in degassed acetonitrile (5 mL). NaOH 1 M (1 eq., 0.16 mL, 0.15 mmol) was added and the mixture was reacted 30 min at room temperature. The mixture was then transferred on a solution of 2-aminoethyldiphenylphosphane gold(I) chloride **A** (1 eq., 70 mg, 0.15 mmol) in dichloromethane (3 mL) at 0 °C. After the end of the addition, the ice bath was removed and the mixture was reacted for 3 h at room temperature. After removal of the solvents under vacuum and redissolution in dichloromethane, the solution was filtered through Celite®. Upon removal of dichloromethane under vacuum, and rinsing with pentane, an off-white product was obtained as a powder (108 mg, 90 % yield). ^{1}H NMR ($CDCl_3$, 300 K, 600.23 MHz): 1.87 (broad s, 2 H, NH_2), 1.94 (s, 3 H, $CH_3C(O)$), 1.98 (s, 3 H, $CH_3C(O)$), 2.01 (s, 3 H, $CH_3C(O)$), 2.07 (s, 3 H, $CH_3C(O)$), 2.69 (m, 2H, P–CH_2), 3.10 (m, 2 H, N–CH_2), 3.76 (dd, 1 H, $^3J_{H–H}$ = 2.4 Hz, $^3J_{H–H}$ = 9.0 Hz, CH_{sugar}), 4.11 (dd, 1 H, $^2J_{H–H}$ = 12.6 Hz, $^3J_{H–H}$ = 2.4 Hz, $CH_{2\text{-}sugar}$), 4.23 (dd, 1 H, $^2J_{H–H}$ = 12.6 Hz, $^3J_{H–H}$ = 9.0 Hz, $CH_{2\text{-}sugar}$), 5.06–5.17

(m, 4 H, 4 CH_{sugar}), 7.47–7.51 (m, 6 H, 4 $CH_{meta\text{-}Ph}$ + 2 $CH_{para\text{-}Ph}$), 7.69–7.75 (m, 4 H, 4 $CH_{ortho\text{-}Ph}$). $^{13}C\{^1H\}$ NMR ($CDCl_3$, 300 K, 150.94 MHz): 20.8 (s, $CH_3C(O)$), 20.9 (s, $CH_3C(O)$), 21.0 (s, $CH_3C(O)$), 21.3 (s, $CH_3C(O)$), 32.1 (d, $^1J_{P-C}$ = 34.7 Hz, CH_2–P), 38.6 (d, $^2J_{P-C}$ = 7.5 Hz, CH_2–NH_2), 63.0 (s, $CH_{2\text{-}sugar}$), 69.1 (s, CH_{sugar}), 74.4 (s, CH_{sugar}), 76.0 (s, CH_{sugar}), 77.9 (s, CH_{sugar}), 83.4 (s, CH_{sugar}), 129.4 (d, $^3J_{P-C}$ = 3.0 Hz, CH_{meta}), 129.5 (d, $^3J_{P-C}$ = 3.0 Hz, CH_{meta}), 130.0 (d, $^1J_{P-C}$ = 13.6 Hz, C_{ipso}), 130.4 (d, $^1J_{P-C}$ = 13.6 Hz, C_{ipso}), 131.8 (s, CH_{para}), 131.9 (s, CH_{para}), 133.4 (d, $^2J_{P-C}$ = 7.5 Hz, CH_{ortho}), 133.5 (d, $^2J_{P-C}$ = 7.5 Hz, CH_{ortho}), 169.8 (s, C(O)), 170.0 (s, C(O)), 170.4 (s, C(O)), 170.9 (s, C(O)). $^{31}P\{^1H\}$ NMR ($CDCl_3$, 300 K, 242.96 MHz): 29.4 (broad s, P–Au–S). IR (ATR, cm^{-1}): 2945, 1740, 1436, 1368, 1218, 1102, 1030, 519, 487, 373, 215. ESI–MS (DCM/MeOH), positive mode exact mass for $[C_{28}H_{35}AuNO_9S.H]^+$ (790.15084): measured *m/z* 790.14896 $[M + H]^+$. Anal. Calc. for $C_{28}H_{35}AuNO_9PS.H_2O$: C, 41.64, H, 4.62, N, 1.73, S, 3.97 %. Found: C, 41.63, H, 4.80, N, 1.73, S, 3.39 %.

*General procedure for the microwave-based coupling reactions (compounds **3** and **5**)*

A microwave 10–mL tube was charged with **1** (1 eq.) and H_2N–CH_2–R (1 eq.) dissolved in distilled acetonitrile. The mixture was reacted in microwave oven (quick heating from room temperature to 80 °C, 850 W, stirring at 600 rpm) at 80 °C (temperature checked by IR probe) for 30 min (50 W, stirring at 600 rpm). After evaporation of the acetonitrile, the product was redissolved in dichloromethane and filtered through Celite®. After partial removal of dichloromethane and addition of diethylether or pentane for **3** and **5,** respectively, the obtained precipitate was filtered and dried under vacuum to give the pure product.

*1-Methyl-3-(4-((diphenylphosphane gold(I) thiolato-β-D-glucose tetraacetate)ethylcarbamoyl)benzyl) imidazole-2-ylidene gold(I) chloride (**3**)*

1 (47 mg, 0.076 mmol), **B** (0.076 mmol, 25 mg), acetonitrile (4 mL). Product as an off-white powder (61 mg, 67 % yield). ^1H NMR ($CDCl_3$, 298 K, 600.23 MHz): 1.92 (s, 3 H, $CH_3C(O)$), 1.96 (s, 3 H, $CH_3C(O)$), 2.03 (s, 3 H, $CH_3C(O)$), 2.06 (s, 3 H, $CH_3C(O)$), 2.85–2.91 (m, 1 H, P–CH_2), 2.97–2.99 (m, 1 H, P–CH_2), 3.73–3.77 (m, 3 H, CH_{sugar} + NH–CH_2), 3.86 (s, 3 H, N–CH_3), 4.08 (d, 1 H, $^2J_{H-H}$ = 10.2 Hz, $CH_{2\text{-}sugar}$), 4.19 (dd, 1 H, $^2J_{H-H}$ = 10.2 Hz, $^3J_{H-H}$ = 4.2 Hz, $CH_{2\text{-}sugar}$), 5.08–5.21 (m, 4 H, 4 CH_{sugar}), 5.34 (d, 1 H, $^2J_{H-H}$ = 15.0 Hz, NCH_2), 5.42 (broad s, 1 H, NCH_2), 6.94 (s, 1 H, CH_{Im}), 6.97 (s, 1 H, $^3J_{H-H}$ = 1.8 Hz, CH_{Im}), 7.31 (broad s, 2 H, 2 $CH_{p\text{-}C6H4}$), 7.42–7.47 (m, 7 H, NH + 4 $CH_{meta\text{-}Ph}$ + 2 $CH_{para\text{-}Ph}$), 7.68–7.71 (m, 6 H, 2 $CH_{p\text{-}C6H4}$ + 4 $CH_{ortho\text{-}Ph}$). $^{13}C\{^1H\}$ NMR ($CDCl_3$, 300 K, 150.94 MHz): 20.8 (s, O(O)C–CH_3), 20.9 (s, O(O)C–CH_3), 21.4 (s, O(O)C–CH_3), 28.1 (d, $^1J_{P-C}$ = 33.9 Hz, CH_2–P), 37.1 (d, $^2J_{P-C}$ = 6.3 Hz, CH_2–NH), 38.4 (s, N–CH_3), 54.4 (s, N–CH_2), 62.9 (s, $CH_{2\text{-}sugar}$), 69.1 (broad s, CH_{sugar}), 74.4 (s, CH_{sugar}), 75.9 (s, CH_{sugar}), 78.0 (broad s, CH_{sugar}), 83.2 (broad s, CH_{sugar}), 120.8 (s, CH_{Im}), 122.5 (s, CH_{Im}), 127.9 (s, $CH_{p\text{-}C6H4}$), 128.1 (s, $CH_{p\text{-}C6H4}$), 129.4 (d, $^2J_{P-C}$ = 10.1 Hz, $CH_{ortho\text{-}Ph}$), 129.5 (d, $^2J_{P-C}$ = 10.1 Hz, $CH_{ortho\text{-}Ph}$), 131.6 (s, $C_{quat\text{-}p\text{-}C6H4}$), 132.0 (s, $CH_{para\text{-}Ph}$), 132.1 (s, $CH_{para\text{-}Ph}$), 133.2 (d, $^3J_{P-C}$ = 13.8 Hz, $CH_{meta\text{-}Ph}$), 133.4 (d, $^3J_{P-C}$ = 13.8 Hz, $CH_{meta\text{-}Ph}$), 134.1 (s, $C_{quat\text{-}p\text{-}C6H4}$), 167.2 (s, C(O)–NH), 169.9 (s, $C_{carbene}$), 170.3 (s, C(O)O), 170.9 (s, C(O)O) $^{31}P\{^1H\}$ NMR ($CDCl_3$, 300 K, 242.96 MHz): 28.3 (broad s, P–Au–S). IR (ATR, cm^{-1}): 3373, 2945, 1744, 1653, 1520, 1436, 1367, 1103, 1034, 520, 483, 373, 327, 217. ESI–MS (DCM/MeOH), positive mode exact mass for $[C_{40}H_{45}Au_2N_3O_{10}SP]^+$ (1184.18888): measured *m/z* 1184.18760 $[M-Cl]^+$.[1] Anal. Calc. for $C_{40}H_{45}AuN_3O_{10}Au_2PSCl{\cdot}2H_2O$: C, 38.24, H, 3.93, N, 3.34, S, 2.55 %. Found: C, 37.83, H, 3.77, N, 3.48, S, 2.08 %.

*1-Methyl-3-{4-[(4′-methyl-2,2′-bipyridin-4-yl) methylcarbamoyl] benzyl}imidazol-2-ylidene gold(I) chloride (**5**)*

1 (1 eq., 77 mg, 0.13 mmol), **C** (1 eq., 0.13 mmol, 25 mg) were dissolved in the tube in acetonitrile (6 mL). The product was obtained as an off-white powder (65 mg, 83 % yield). ^1H NMR ($CDCl_3$, 298 K, 300.13 MHz): 2.44 (s, 3 H, Me-Pyr), 3.85 (s, 3 H, N-Me), 4.71 (d, 2 H, $^3J_{H-H}$ = 6.0 Hz, CH_2–NH), 5.38 (s, 2 H, CH_2–N), 6.83 (broad s, 1 H, NH), 6.89 (d, 1 H, $^3J_{H-H}$ = 1.8 Hz, CH_{Im}), 6.95 (d, 1 H, $^3J_{H-H}$ = 1.8 Hz, CH_{Im}), 7.13 (d, 1 H, $^3J_{H-H}$ = 4.5 Hz, CH_{bipy}), 7.28 (d, 1 H, $^3J_{H-H}$ = 4.8 Hz, CH_{bipy}), 7.35 (d, 2 H, $^3J_{H-H}$ = 8.1 Hz, 2 $CH_{p\text{-}C6H4}$), 7.81 (d, 2 H, $^3J_{H-H}$ = 8.1 Hz, 2 $CH_{p\text{-}C6H4}$), 8.21 (s, 1 H, CH_{bipy}), 8.34 (s, 1 H, CH_{bipy}), 8.49 (d, 1 H, $^3J_{H-H}$ = 4.8 Hz, CH_{bipy}), 8.60 (d, 1 H, $^3J_{H-H}$ = 4.8 Hz, CH_{bipy}). $^{13}C\{^1H\}$ NMR ($CDCl_3$, 300 K, 125.77 MHz): 21.2 (s, CH_3–Pyr), 38.4 (s, CH_3–N), 43.2 (s, CH_2–NH), 54.5 (s, CH_2–N), 119.8 (s, CH_{bipy}), 120.5 (s, CH_{Im}), 122.2 (s, CH_{bipy}), 122.5 (s, CH_{Im} + CH_{bipy}), 124.9 (s, CH_{bipy}), 127.9 (s, $CH_{p\text{-}C6H4}$), 128.1 (s, $CH_{p\text{-}C6H4}$), 134.4 (s, C_{quat}–CH_2), 138.7 (s, C_{quat}–C(O)), 148.2 (s, C^4–$C^{4'}$), 148.3 (s, C^4–$C^{4'}$), 148.9 (s, CH_{bipy}), 149.6 (s, CH_{bipy}), 155.6 (s, $C^{2'}$), 156.7 (s, C^2), 166.9 (s, C(O)), 172.0 (s, $C_{carbene}$). FT-IR (ATR, cm^{-1}): 3338, 3108, 3060, 2929, 1647, 1596, 1535, 1498, 1464, 1436, 1410, 1305, 1236, 1190, 1109, 327. ESI–MS (CH_2Cl_2/MeOH), positive mode exact mass

[1] No signal corresponding to disproportionation or exchange phenomena was observed on HRMS spectrum.

for $[C_{24}H_{23}AuClN_5ONa]^+$ (652.11543): measured *m/z* 652.11436 $[M+Na]^+$. Anal. Calc. for $C_{24}H_{23}AuN_5Cl$: C, 45.76, H, 3.68, N, 11.12 %. Found: C, 45.79, H, 3.67, N, 10.40 %.

*1-Methyl-3-(4-((diphenylphosphane gold(I) thiolato-β-D-glucose tetraacetate)ethylcarbamoyl) benzyl)imidazole-2-ylidene gold(I) thiolato-β-D-glucose tetraacetate (**4**)*

A Schlenk tube was charged under argon with thio-β-D-glucose tetraacetate (2 eq., 50 mg, 0.139 mmol) dissolved in degassed acetone (3 mL). NaOH 1 M (2 eq., 0.14 mL, 0.139 mmol) was added and the mixture and reacted 30 min at room temperature in the dark. The mixture was then transferred on a solution of **2** (1 eq., 62 mg, 0.069 mmol) in degassed acetone (5 mL) at 0 °C. After the end of the addition, the ice bath was removed and the mixture was reacted for 3 h at room temperature in the dark. After removal of the acetone under vacuum and redissolution in dichloromethane, the solution was filtered through Celite®. Upon concentration under reduced pressure, and addition of a large amount of pentane, an off-white precipitate formed which after drying under vacuum gave the product with two molecules of water as a white powder (85 mg, 79 % yield). ^{1}H NMR ($CDCl_3$, 300 K, 300.13 MHz): 1.91 (s, 6 H, 2 × O(O)C–CH_3), 1.93 (s, 6 H, 2 × O(O)C–CH_3), 1.99 (s, 6 H, 2 × O(O)C–CH_3), 2.04 (s, 6 H, 2 × O(O)C–CH_3), 2.79–2.87 (m, 1 H, CH_2–P), 2.99–3.08 (m, 1 H, CH_2–P), 3.73–3.82 (m, 4 H, CH_2–NH + 2 × O–CH_{sugar}–CH_2), 3.86 (s, 3 H, N–CH_3), 4.07 (d, 2 H, $^2J_{H–H}$ = 10.2 Hz, 2 × $CH_{2\text{-}sugar}$), 4.17 (dd, 1 H, $^2J_{H–H}$ = 10.2 Hz, $^3J_{H–H}$ = 4.8 Hz, 2 × $CH_{2\text{-}sugar}$), 5.09 (broad s, 8 H, 2 × 4 CH_{sugar}), 5.34 (d, $^2J_{H–H}$ = 15.3 Hz, $CH_{2\text{-}Bz}$), 5.50 (d, $^2J_{H–H}$ = 15.3 Hz, $CH_{2\text{-}Bz}$), 6.90 (d, 1 H, $^3J_{H–H}$ = 1.8 Hz, CH_{Im}), 6.93 (d, 1 H, $^3J_{H–H}$ = 1.8 Hz, CH_{Im}), 7.34 (d, 2 H, $^3J_{H–H}$ = 8.4 Hz, 2 × $CH_{p\text{-}C6H4}$), 7.40–7.43 (m, 6 H, 2 × $CH_{para\text{-}Ph}$ + 2 × 2 × $CH_{ortho\text{-}Ph}$), 7.66 (broad t, $^3J_{H–H}$ = 3.6 Hz, NH), 7.69–7.81 (m, 6 H, 2 × $CH_{p\text{-}C6H4}$ + 2 × 2 × $CH_{meta\text{-}Ph}$). ^{13}C{^{1}H} NMR ($CDCl_3$, 300 K, 125.77 MHz): 20.8 (s, O(O)C–CH_3), 20.9 (s, O(O)C–CH_3), 21.3 (s, O(O)C–CH_3), 28.0 (d, $^1J_{P–C}$ = 33.9 Hz, CH_2–P), 37.2 (d, $^2J_{P–C}$ = 6.3 Hz, CH_2–NH), 38.1 (s, N–CH_3), 54.2 (s, N–CH_2), 62.9 (s, $CH_{2\text{-}sugar}$), 69.1 (broad s, CH_{sugar}), 74.3 (s, CH_{sugar}), 75.8 (s, CH_{sugar}), 78.0 (broad s, CH_{sugar}), 83.3 (broad s, CH_{sugar}), 120.6 (s, CH_{Im}), 122.4 (s, CH_{Im}), 127.9 (s, $CH_{p\text{-}C6H4}$), 128.0 (s, $CH_{p\text{-}C6H4}$), 129.3 (d, $^2J_{P–C}$ = 10.1 Hz, $CH_{ortho\text{-}Ph}$), 129.4 (d, $^2J_{P–C}$ = 10.1 Hz, $CH_{ortho\text{-}Ph}$), 129.8 (d, $^1J_{P–C}$ = 25.2 Hz, $CH_{ipso\text{-}Ph}$), 130.2 (d, $^1J_{P–C}$ = 25.2 Hz, $CH_{ipso\text{-}Ph}$), 131.8 (d, $^4J_{P–C}$ = 2.5 Hz, $CH_{para\text{-}Ph}$), 131.9 (d, $^4J_{P–C}$ = 2.5 Hz, $CH_{para\text{-}Ph}$), 133.1 (d, $^3J_{P–C}$ = 13.8 Hz, $CH_{meta\text{-}Ph}$), 133.4 (d, $^3J_{P–C}$ = 13.8 Hz, $CH_{meta\text{-}Ph}$), 134.1 (s, $C_{quat\text{-}p\text{-}C6H4}$), 139.1 (s, $C_{quat\text{-}p\text{-}C6H4}$), 167.1 (s, C(O)–NH), 169.9 (s, $C_{carbene}$), 170.2 (s, C(O)O), 170.8 (s, C(O)O). ^{31}P{^{1}H} NMR ($CDCl_3$, 300 K, 202.45 MHz): 30.7 (broad s, P–Au–S). FT-IR (ATR, cm^{-1}): 1740, 1658, 1534, 1435, 1367, 1217, 1030, 602, 372, 216. ESI–MS (H_2O/MeOH), positive mode exact mass for $[C_{54}H_{64}Au_2N_3O_{19}PS_2Na]^+$ (1570.25363): measured *m/z* 1570.26001 $[M + Na]^+$ (see footnote 1). Anal. Calc. for $C_{54}H_{64}Au_2N_3O_{19}PS_2.2H_2O$: C, 40.94, H, 4.33, N, 2.65, S, 4.05 %. Found: C, 40.53, H, 4.31, N, 2.84, S, 3.14 %.

*(4,4′-Dimethyl-2,2′-bipyridine) copper(II) dichloride (**6**)*

A Schlenk tube was charged under argon with $CuCl_2.2H_2O$ (1 eq., 92 mg, 0.542 mmol) in methanol (3 mL) and transferred on 4,4′-dimethyl-2,2′-bipyridine (1 eq., 100 mg, 0.542 mmol) dissolved in dichloromethane (6 mL). The mixture was reacted for 3 h at room temperature under argon during which period of time a green precipitate formed. After removal of the solvents by filtration and drying under vacuum, the product was obtained as a green powder. (168 mg, 97 % yield). FT-IR (ATR, cm^{-1}): 3378, 3109, 2941, 1653, 1615, 1562, 1534, 1499, 1467, 1418, 1360, 1289, 1230, 1194, 1022, 831, 738, 425, 316, 303, 184, 167, 155, 137. ESI–MS (DMSO/MeOH), positive mode exact mass for $[C_{12}H_{12}N_2CuCl]^+$ (281.99795): measured *m/z* 281.99656 $[M\text{-}Cl]^+$. Anal. Calc. for $C_{12}H_{12}CuN_2Cl_2$: C, 45.23, H, 3.80, N, 8.79 %. Found: C, 45.14, H, 4.10 N, 8.78 %.

*[(4,4′-Methyl-2,2′-bipyridine)(p-cymene) ruthenium(II) chloride] hexafluorophosphate (**7**)*

A Schlenk tube was charged under argon with 4,4′-dimethyl-2,2′-bipyridine (1 eq., 50 mg, 0.27 mmol), $[(p\text{-cymene})RuCl_2]_2$ (0.5 eq., 83 mg, 0.14 mmol) and KPF_6 (4 eq., 200 mg, 1.06 mmol) dissolved in distilled acetone (8 mL). The mixture was reacted overnight at room temperature under argon. After removal of the acetone under vacuum and redissolution in dichloromethane, the solution was filtered through Celite®. Upon concentration under reduced pressure, and addition of diethylether (10 mL) and pentane (20 mL), a yellow precipitate formed which after drying under vacuum gave the pure product as a yellow powder (158 mg, 97 % yield). ^{1}H NMR (acetone-d6, 300 K, 300.13 MHz): 1.08 (d, 3 H, $^3J_{H–H}$ = 6.0 Hz, 2 × CH_3–CH), 2.29 (s, 3 H, $CH_{3\text{-}p\text{-cymene}}$), 2.63 (s, 6 H, 2 × $CH_{3\text{-bipy}}$), 2.77 (m, 1 H, $CH(CH_3)_2$), 5.92 (d, 2 H, $^3J_{H–H}$ = 6.0 Hz, 2 × $CH_{arom\text{-}p\text{-cymene}}$), 6.17 (d, 2 H, $^3J_{H–H}$ = 6.0 Hz, 2 × $CH_{arom\text{-}p\text{-cymene}}$), 7.62 (dd, 2 H, $^3J_{H–H}$ = 6.0 Hz, $^4J_{H–H}$ = 2.1 Hz, $CH^{5,5'}$), 7.96 8.43 (s, 2 H, $CH^{3,3'}$), 9.38 (d, 2 H, $^3J_{H–H}$ = 6.3 Hz, $CH^{6,6'}$). FT-IR (ATR, cm^{-1}): 1658, 1620, 1531, 1499, 1467, 1417, 1293, 1238, 831, 740, 556, 285.

*[(1-Methyl-3-(4-((4′-methyl-2,2′-bipyridin-4-yl) methylcarbamoyl)benzyl)imidazol-2-ylidene gold(I) chloride]-[copper(II) dichloride] (**8**)*

A Schlenk tube was charged under argon with **5** (1 eq., 50 mg, 0.079 mmol), $CuCl_2.2H_2O$ (1 eq., 14 mg, 0.079 mmol) dissolved in distilled acetone (3 mL). The mixture was reacted for 3 h at room temperature under argon during which period of time a green precipitate formed. After removal of the acetone by filtration and drying under vacuum, the product with a molecule of water was obtained as a green powder. (50 mg, 97 % yield). FT-IR (ATR, cm^{-1}): 3378, 3109, 2941, 1653, 1615, 1562, 1534, 1499, 1467, 1418, 1360, 1289, 1230, 1194, 1022, 831, 738, 424, 328, 310, 286, 134. ESI–MS (DMSO/MeOH), positive mode exact mass for $[C_{24}H_{23}AuN_5OCuCl_2]^+$ (727.02357): measured *m/z* 727.02078 $[M-Cl]^+$. Anal. Calc. for $C_{24}H_{23}AuCuN_5Cl_3.H_2O$: C, 36.84, H, 3.22, N, 8.95 %. Found: C, 36.83, H, 2.68, N, 8.95 %.

*[(1-Methyl-3-(4-((4′-methyl-2,2′-bipyridin-4-yl) methylcarbamoyl)benzyl)imidazol-2-ylidene gold(I) chloride]-[(p-cymene) ruthenium(II) chloride] hexafluorophosphate (**9**)*

A Schlenk tube was charged under argon with **5** (1 eq., 50 mg, 0.079 mmol), $[(p\text{-cymene})RuCl_2]_2$ (0.5 eq., 24 mg, 0.040 mmol) and KPF_6 (4 eq., 58 mg, 0.318 mmol) dissolved in distilled acetone (5 mL). The mixture was reacted overnight at room temperature under argon. After removal of the acetone under vacuum and redissolution in dichloromethane, the solution was filtered through Celite®. Upon concentration under reduced pressure, and addition of diethylether (10 mL) and pentane (20 mL), a yellow precipitate formed which after drying under vacuum gave the pure product as a yellow powder (79 mg, 95 % yield). ^{1}H NMR (acetone-d6, 300 K, 600.23 MHz): 1.08 (d, 3 H, $^3J_{H-H}$ = 6.0 Hz, CH_3–CH), 1.09 (d, 3 H, $^3J_{H-H}$ = 6.0 Hz, CH_3–CH), 2.28 (s, 3 H, $CH_{3\text{-}p\text{-cymene}}$), 2.59 (s, 3 H, $CH_{3\text{-bipy}}$), 2.77 (m, 1 H, $CH(CH_3)_2$), 3.88 (s, 3 H, CH_3–N), 4.86 (pseudo t, 2 H, $^3J_{H-H}$ = 6.3 Hz, CH_2–NH), 5.53 (s, 2 H, CH_2–N), 5.94 (pseudo t, 2 H, $^3J_{H-H}$ = 6.0 Hz, 2 $CH_{arom\text{-}p\text{-cymene}}$), 6.18 (pseudo t, 2 H, $^3J_{H-H}$ = 6.0 Hz, 2 $CH_{arom\text{-}p\text{-cymene}}$), 7.42 (d, 1 H, $^3J_{H-H}$ = 1.8 Hz, CH_{Im}), 7.48 (d, 1 H, $^3J_{H-H}$ = 1.8 Hz, CH_{Im}), 7.53 (d, 2 H, $^3J_{H-H}$ = 8.4 Hz, 2 $CH_{arom\text{-}p\text{-C6H4}}$), 7.62 (d, 1 H, $^3J_{H-H}$ = 6.0 Hz, $CH^{5'}$), 7.72 (d, 1 H, $^3J_{H-H}$ = 6.0 Hz, CH^5), 7.96 (d, 2 H, $^3J_{H-H}$ = 8.4 Hz, 2 $CH_{arom\text{-}p\text{-C6H4}}$), 8.43 (s, 1 H, $CH^{3'}$), 8.55 (m, 2 H, NH + CH^3), 9.39 (d, 1 H, $^3J_{H-H}$ = 6.0 Hz, $CH^{6'}$), 9.46 (d, 1 H, $^3J_{H-H}$ = 6.0 Hz, CH^6). $^{13}C\{^1H\}$ NMR (acetone-d6, 300 K, 125.77 MHz): 18.8 (s, $CH_{3\text{-}p\text{-cymene}}$), 21.2 (s, $CH_{3\text{-bipy}}$), 22.2 (s, CH_3–CH), 22.3 (s, CH_3–CH), 31.9 (s, CH–$(CH_3)_2$), 38.5 (s, N–CH_3), 43.2 (s, CH_2–NH), 54.7 (s, N–CH_2), 85.1 (s, $CH_{arom\text{-}p\text{-cymene}}$), 85.3 (s, $CH_{arom\text{-}p\text{-cymene}}$), 87.3 (s, $CH_{arom\text{-}p\text{-cymene}}$), 87.4 (s, $CH_{arom\text{-}p\text{-cymene}}$), 104.3 (s, $C_{quat\text{-}p\text{-cymene}}$), 105.8 (s, $C_{quat\text{-}p\text{-cymene}}$), 122.4 (s, CH_{Im}), 122.9 (s, CH_{bipy}), 123.9 (s, CH_{Im}), 125.3 (s, CH_{bipy}), 126.7 (s, CH_{bipy}), 128.8 (s, 4 $CH_{p\text{-C6H4}}$), 129.3 (s, CH_{bipy}), 134.9 (s, $C_{quat\text{-}p\text{-C6H4}}$), 141.3 (s, $C_{quat\text{-}p\text{-C6H4}}$), 153.4 (s, $C_{quat\text{-bipy}}$), 154.7 (s, $C_{quat\text{-bipy}}$), 155.3 (s, $C_{quat\text{-bipy}}$), 155.7 (s, $C_{quat\text{-bipy}}$), 155.8 (s, CH_{bipy}), 156.2 (s, CH_{bipy}), 167.5 (s, C(O)), 172.4 (s, $C_{carbene}$). FT-IR (ATR, cm^{-1}): 1658, 1620, 1531, 1499, 1467, 1417, 1293, 1238, 831, 740, 556, 328, 284. ESI–MS (MeOH), positive mode exact mass for $[C_{34}H_{37}AuN_5ORuCl_2]^+$ (900.10819): measured *m/z* 900.11158 $[M-PF_6]^+$. Anal. Calc. for $C_{34}H_{43}AuRuN_5Cl_2PF_6$: C, 38.83, H, 4.12, N, 6.66 %. Found: C, 38.70, H, 3.77, N, 6.25 %.

*(1-Methyl-3-(4-((4′-methyl-2,2′-bipyridin-4-yl) methylcarbamoyl)benzyl)imidazol-2-ylidene gold(I) (thiolato-β-D-glucose tetraacetate) (**10**)*

A Schlenk tube was charged under argon with thio-β-D-glucose tetraacetate (1 eq., 29 mg, 0.079 mmol) dissolved in degassed acetone (2 mL). NaOH 1 M (1 eq., 0.08 mL, 0.079 mmol) was added and the mixture was reacted 30 min at room temperature in the dark. The mixture was then transferred onto a solution of **5** (1 eq., 49 mg, 0.079 mmol,) in degassed acetone (2 mL) at 0 °C. After the end of the addition, the ice bath was removed and the mixture was reacted for 3 h at room temperature in the dark. After removal of the acetone under vacuum and redissolution in dichloromethane, the solution was filtered through Celite®. Upon concentration under reduced pressure, and addition of pentane (20 mL), an off-white precipitate formed which after drying under vacuum gave the product with one molecule of water as a white powder (46 mg, 61 % yield). ^{1}H NMR ($CDCl_3$, 300 K, 300.13 MHz): 1.85 (s, 3 H, $CH_3C(O)$), 1.87 (s, 3 H, $CH_3C(O)$), 1.88 (s, 3 H, $CH_3C(O)$), 2.08 (s, 3 H, $CH_3C(O)$), 2.43 (s, 3 H, $CH_{3\text{-Bipy}}$), 3.68-3.71 (m, 1 H, CH_{sugar}), 3.85 (s, 3 H, NCH_3), 4.05-4.08 (m, 2 H, CH_2–NH), 4.66 (dd, 1H, $^2J_{H-H}$ = 15.6 Hz, $^3J_{H-H}$ = 5.7 Hz, $CH_{2\text{-sugar}}$), 4.79 (dd, 1H, $^2J_{H-H}$ = 15.6 Hz, $^3J_{H-H}$ = 5.7 Hz, $CH_{2\text{-sugar}}$), 4.93–5.11 (m, 4 H, 4 × CH_{sugar}), 5.33 (d, 1 H, $^2J_{H-H}$ = 15.3 Hz, NCH_2), 5.75 (d, 1 H, $^2J_{H-H}$ = 15.3 Hz, NCH_2), 6.94 (d, 1 H, $^3J_{H-H}$ = 1.8 Hz, CH_{Im}), 6.99 (d, 1 H, $^3J_{H-H}$ = 1.8 Hz, CH_{Im}), 7.12 (dd, 1 H, $^3J_{H-H}$ = 5.1 Hz, $^4J_{H-H}$ = 0.9 Hz, $CH^{5'}$), 7.30 (dd, 1 H, $^3J_{H-H}$ = 5.1 Hz, $^4J_{H-H}$ = 1.5 Hz, CH^5), 7.54 (d, 2 H, $^3J_{H-H}$ = 8.4 Hz, 2 × $CH_{p\text{-C6H4}}$), 7.70 (broad t, 1 H, $^3J_{H-H}$ = 5.1 Hz, NH), 7.95 (d, 2 H, $^3J_{H-H}$ = 8.4 Hz, 2 × $CH_{p\text{-C6H4}}$), 8.21 (s, 1 H, $CH^{3'}$), 8.37 (s, 1 H, $CH^{3'}$), 8.48 (d, 1 H, $^3J_{H-H}$ = 5.1 Hz, $CH^{6'}$), 8.60 (d, 1 H, $^3J_{H-H}$ = 5.1 Hz, CH^6). $^{13}C\{^1H\}$ NMR ($CDCl_3$, 300 K, 125.77 MHz): 20.7 (s, $CH_3C(O)$), 20.8 (s, $CH_3C(O)$), 20.9 (s, $CH_3C(O)$), 21.4 (s, $CH_3C(O)$), 21.5 (s, $CH_{3\text{-bipy}}$), 38.2 (s, CH_3–N), 43.4 (s, $CH_{2\text{-sugar}}$), 54.2 (s, CH_2–NH),

63.3 (s, CH_{sugar}), 69.8 (s, CH_{sugar}), 74.4 (s, CH_{sugar}), 75.6 (s, CH_{sugar}), 78.6 (s, CH_{sugar}), 83.6 (s, CH_{sugar}), 120.2 (s, CH^3), 120.9 (s, CH_{Im}), 122.2 (s, $CH^{3'}$), 122.4 (s, CH_{Im}), 122.8 (s, CH^5), 125.1 (s, $CH^{5'}$), 128.0 (s, $CH_{p\text{-C6H4}}$), 128.3 (s, $CH_{p\text{-C6H4}}$), 134.6 (s, $C_{quat\text{-}p\text{-C6H4}}$), 139.9 (s, $C_{quat\text{-}p\text{-C6H4}}$), 148.4 (s, C^4_{quat}), 148.9 (s, $C^{4'}_{quat}$), 149.2 (s, $CH^{6'}$), 149.6 (s, CH^6), 155.8 (s, C^2_{quat}), 156.8 (s, $C^{2'}_{quat}$), 167.3 (s, C(O)–NH), 170.3 (s, C(O)O), 170.9 (s, C(O)O), 171.0 (s, C(O)O), 184.3 (s, $C_{carbene}$). FT-IR (ATR, cm^{-1}): 3374, 2944, 1743, 1657, 1597, 1535, 1503, 1462, 1433, 1368, 1223, 1032, 607, 374. ESI–MS (MeOH), positive mode exact mass for $[C_{38}H_{43}AuN_5O_{10}SH]^+$ (958.23907): measured *m/z* 958.23529 $[M + H]^+$. ESI–MS (MeOH), positive mode exact mass for $[C_{38}H_{43}AuN_5O_{10}SNa]^+$ (980.22101): measured *m/z* 980.21460 $[M+Na]^+$. Anal. Calc. for $C_{38}H_{42}AuN_5O_{10}S.H_2O$: C, 46.77, H, 4.54, N, 7.18, S, 3.27 %. Found: C, 46.59, H, 4.37, N, 6.97, S, 3.10 %.

*[(1-Methyl-3-(4-((4′-methyl-2,2′-bipyridin-4-yl) methylcarbamoyl)benzyl)imidazol-2-ylidene gold(I) (thiolato-β-D-glucose tetraacetate)]-[(p-cymene) ruthenium(II) chloride] hexafluorophosphate (**11**)*

A Schlenk tube was charged under argon with **10** (1 eq., 30 mg, 0.031 mmol), $[(p\text{-cymene})RuCl_2]_2$ (0.5 eq., 10 mg, 0.016 mmol) and KPF_6 (4 eq., 23 mg, 0.125 mmol) dissolved in distilled acetone (3 mL). The mixture was reacted for 4 h at room temperature under argon. After removal of the acetone under vacuum and redissolution in dichloromethane, the solution was filtered through Celite®. Upon concentration under reduced pressure, and addition of diethylether (10 mL) and pentane (20 mL), a yellow precipitate formed which after drying under vacuum gave the product as a mixture of the two possible diastereoisomers in ratio 50/50 as a yellow powder. The product was isolated as an adduct with two molecules of water (42 mg, 92 % yield). ^{1}H NMR (acetone-d6, 300 K, 600.23 MHz): 1.07 (m, 6 H, 2 $CH_{3\text{-iPr}}$), 1.23 (m, 6 H, 2 $CH_{3\text{-iPr}}$), 1.82 (s, 3 H, $CH_3C(O)$), 1.93 (s, 3 H, $CH_3C(O)$), 1.93 (s, 3 H, $CH_3C(O)$), 1.97 (s, 3 H, $CH_3C(O)$), 2.00 (s, 6 H, 2 $CH_3C(O)$), 2.03 (s, 3 H, $CH_3C(O)$), 2.12 (broad s, 3 H, $CH_3C(O)$), 2.16 (broad s, 3 H, $CH_3C(O)$), 2.26 (s, 3 H, $CH_{3\text{-}p\text{-cymene}}$), 2.42 (s, 3 H, $CH_{3\text{-}p\text{-cymene}}$), 2.56 (s, 3 H, $CH_{3\text{-bipy}}$), 2.79 (s, 3 H, $CH_{3\text{-bipy}}$), 3.89 (broad m, 6 H, 2 NCH_3), 4.07-4.11 (m, 3 H, 3 CH_{sugar}), 4.19 (dd, 1 H, $^2J_{H–H}$ = 11.4 Hz, $^3J_{H–H}$ = 4.8 Hz, $CH_{2\text{-sugar}}$), 4.55 (broad d, 1 H, $^3J_{H–H}$ = 6.6 Hz, CH_{sugar}), 4.70 (d, 2 H, $^3J_{H–H}$ = 6.0 Hz, CH_2–NH), 4.84 (broad m, 2 H, CH_2–NH), 5.06 (t, 1 H, $^3J_{H–H}$ = 9.9 Hz, CH_{sugar}), 5.12 (t, 1 H, $^3J_{H–H}$ = 9.9 Hz, CH_{sugar}), 5.23-5.58 (m, 3 H, 3 CH_{sugar}), 5.36 (broad m, 2 H, 2 CH_{sugar}), 5.42 (d, 1 H, $^3J_{H–H}$ = 9.9 Hz, CH_{sugar}), 5.52 (m, 4 H, 2 CH_2–N), 5.85 (broad s, 1 H, CH_{sugar}), 5.91 (d, 4 H, 2 × 2 $CH_{arom\text{-}p\text{-cymene}}$), 6.16 (m, 4 H, 2 × 2 $CH_{arom\text{-}p\text{-cymene}}$), 7.22 (d, 1 H, $^3J_{H–H}$ = 4.8 Hz, CH_{bipy}), 7.37 (d, 1 H, $^3J_{H\text{-}H}$ = 4.2 Hz, CH_{bipy}), 7.41 (s, 2 H, 2 CH_{Im}), 7.48 (s, 1 H, CH_{Im}), 7.52 (m, 5 H, CH_{Im} + 2 × 2 $CH_{p\text{-C6H4}}$), 7.60 (d, 1 H, $^3J_{H–H}$ = 5.4 Hz, CH_{bipy}), 7.70 (d, 1 H, $^3J_{H–H}$ = 5.4 Hz, CH_{bipy}), 7.88 (d, 3 H, $^3J_{H–H}$ = 7.2 Hz, 3 $CH_{arom\text{-}p\text{-C6H4}}$), 7.96 (d, 1 H, $^3J_{H–H}$ = 7.2 Hz, $CH_{arom\text{-}p\text{-C6H4}}$), 8.28 (s, 1 H, CH_{bipy}), 8.39 (s, 1 H, CH_{bipy}), 8.41 (d, 1 H, $^3J_{H–H}$ = 6.0 Hz, NH), 8.45 (m, 3 H, 3 CH_{bipy}), 8.53 (m, 1 H, NH), 8.57 (d, 1 H, $^3J_{H–H}$ = 5.4 Hz, CH_{bipy}), 9.38 (d, 1 H, $^3J_{H–H}$ = 5.4 Hz, CH_{bipy}), 9.44 (d, 1 H, $^3J_{H–H}$ = 5.4 Hz, CH_{bipy}). $^{13}C\{^1H\}$ NMR (acetone-d6, 300 K, 150.94 MHz): 18.4 (broad s, $CH_{3\text{-}p\text{-cymene}}$), 18.8 (s, $CH_{3\text{-}p\text{-cymene}}$), 20.6 (s, $CH_{3\text{-bipy}}/CH_3C(O)$), 21.0 (s, $CH_{3\text{-bipy}}/CH_3C(O)$), 21.1 (s, $CH_{3\text{-bipy}}/CH_3C(O)$), 22.3 (s, $CH_{3\text{-iPr}}$), 31.8 (s, CH_{iPr}), 38.5 (s, NCH_3), 43.2 (s, CH_2–NH), 43.3 (s, CH_2–NH), 54.6 (broad s, NCH_2), 62.9 (s, $CH_{2\text{-sugar}}$), 63.0 (s, $CH_{2\text{-sugar}}$), 69.1 (s, CH_{sugar}), 69.2 (s, CH_{sugar}), 74.4 (broad s, CH_{sugar}), 76.9 (s, CH_{sugar}), 77.6 (s, CH_{sugar}), 82.2 (s, CH_{sugar}), 85.2 (s, $CH_{arom\text{-}p\text{-cymene}}$), 85.3 (s, $CH_{arom\text{-}p\text{-cymene}}$), 87.4 (s, $CH_{arom\text{-}p\text{-cymene}}$), 104.3 (s, $C_{quat\text{-}p\text{-cymene}}$), 105.8 (s, $C_{quat\text{-}p\text{-cymene}}$), 120.2 (s, CH_{bipy}), 122.4 (s, CH_{bipy}), 122.9 (s, CH_{bipy}), 123.0 (s, CH_{bipy}), 123.4 (s, CH_{bipy}), 123.5 (s, CH_{bipy}), 124.4 (s, CH_{bipy}), 125.2 (s, CH_{bipy}), 125.7 (s, CH_{bipy}), 126.7 (s, CH_{bipy}), 126.8 (s, CH_{bipy}), 128.3 (s, $CH_{p\text{-C6H4}}$), 128.8 (s, $CH_{p\text{-C6H4}}$), 129.3 (s, $CH_{p\text{-C6H4}}$), 134.8 (s, $C_{quat\text{-arom}}$), 135.4 (s, $C_{quat\text{-arom}}$), 141.2 (broad s, $C_{quat\text{-arom}}$), 148.9 (s, $C_{quat\text{-arom}}$), 149.8 (s, CH_{bipy}), 150.1 (s, CH_{bipy}), 150.5 (s, $C_{quat\text{-arom}}$), 153.3 (s, $C_{quat\text{-arom}}$), 154.5 (s, $C_{quat\text{-arom}}$), 155.3 (s, $C_{quat\text{-arom}}$), 155.7 (s, $C_{quat\text{-arom}}$), 155.8 (s, CH_{bipy}), 156.2 (s, CH_{bipy}), 156.6 (s, $C_{quat\text{-arom}}$), 157.1 (s, $C_{quat\text{-arom}}$), 167.2 (s, C(O)N), 167.5 (s, C(O)N), 170.0 (s, C(O)O), 170.4 (s, C(O)O), 170.7 (s, C(O)O), 170.8 (s, C(O)O), $C_{carbene}$ was not observed. FT-IR (ATR, cm^{-1}): 3430, 2927, 1746, 1657, 1621, 1534, 1501, 1466, 1432, 1370, 1225, 1037, 833, 557, 375, 287. ESI–MS (MeCN), positive mode exact *mass* for $[C_{48}H_{56}AuN_5O_{10}SRuCl]^+$ (1228.21496): measured *m/z* 1228.21411 $[M\text{-}PF_6]^+$. Anal. Calc. for $C_{48}H_{56}AuClN_5O_{10}SRuPF_6.2H_2O$: C, 40.90, H, 4.29, N, 4.97, S, 2.27 %. Found: C, 40.63, H, 4.27, N, 4.77, S, 2.24 %.

Antiproliferative assay

The human ovarian cancer cell line A2780 was obtained from the European Centre of Cell Cultures ECACC (Salisbury, UK) and cultured in RPMI medium containing GlutaMaxI supplemented with 10 % FBS and 1 % penicillin/streptomycin (Invitrogen); lung carcinoma cells (A549; ATCC) and ovarian adenocarcinoma cells (SKOV-3; ATCC) were cultivated in DMEM medium, added with GlutaMaxI (containing 10 % FBS and 1 % penicillin/streptomycin. Cells were grown at 37 °C in a humidified atmosphere of 95 % of air and 5 % CO_2 (Heraeus, Germany). For evaluation of growth inhibition, cells were seeded in 96-well

plates and grown for 24 h in complete medium. Following 72-h drug exposure, 3-(4,5-dimethylthiazol-2-yl)-2,5-diphenyltetrazolium bromide (MTT) was added to the cells (0.25 mg $mL^{-1)}$ incubated for 2 h, then the culture medium was removed and the violet formazan dissolved in DMSO. The optical density of each well was quantified in tetraplicates at 540 nm using a multi-well plate reader, and the percentage of surviving cells was calculated from the ratio of absorbance of treated to untreated cells. The IC_{50} value was calculated as the concentration reducing the proliferation of the cells by 50 % and it is presented as a mean (±SE) of at least three independent experiments.

Preparation of rat precision-cut tissue slices (PCTS) and toxicity studies ex vivo

Animal model

Male Wistar rats (Charles River, Kissles, Germany) of 250-450 g were housed under a 12-h dark/light cycle at constant humidity and temperature. Animals were permitted free access to tap water and standard lab chow. All experiments were approved by the committee for care and use of laboratory animals of the University of Groningen and were performed according to strict governmental and international guidelines.

Slices preparation and incubation

Rat liver was excised under 5 % isoflurane/95 % O_2 anaesthesia and placed into ice-cold University of Wisconsin (UW) organ preservation solution. PCLS were prepared as previously described in literature. Briefly, cylindrical cores were generated by drilling a hollow bit (diameter = 5 mm) into the liver. These cores were stored in ice-cold UW until they were sliced with a pre-cooled Krumdieck tissue slicer in ice-cold Krebs–Henseleit buffer saturated with carbogen (95 % O_2/5 % CO_2). PCLS (average of 5 mm diameter, 250 μm thickness and 5 mg wet weight) were stored in ice-cold UW solution until incubation [66, 70]. Incubation of PCLS took place in Williams medium E glutamax (WME, Gibco) supplemented with additional D-glucose monohydrate (1.375 g/500 mL) and gentamicin solution (50 mg/mL; 500 μL/500 mL). The medium (1.3 mL/well) was transferred to 12-well culture plates (Greiner bio-one) and the plates prewarmed (37 °C) and oxygenated (95 % O_2/5 % CO_2) for at least 30 min. The slices were then transferred to the incubation plates (1 slice/well) and incubated for 1 h at 37 °C and stirred at 90 rpm in carbogen atmosphere. This preincubation allows the PCLS to restore their ATP levels. The slices were transferred to new incubation plates with fresh preincubated WME and the test compounds were added at different concentrations (0, 1, 5, 15 and 30 μM) and incubated for 24 h. Stock solutions (10 mM) of metal compounds were freshly prepared prior to the assay using DMSO. The final DMSO concentration was always ≤0.5 % to exclude DMSO toxicity. Afterwards, slices were collected in 1 ml of 70 % ethanol/2 mM ethylenediaminetetraacetic acid (EDTA), quick-frozen in liquid nitrogen and stored at −80 °C until ATP and protein determinations.

ATP assay determination

The viability of the slices was determined by measuring the ATP content using the ATP Bioluminescence Assay kit CLS II (Roche). Luciferase catalyses the reaction: ATP + D-luciferin + O_2 → oxyluciferin + PP_i + AMP + CO_2 + light. The light output is directly proportional to the ATP concentration and dependent on the amount of luciferase present. The resulting green light has an emission maximum of 562 nm and can be measured with spectroscopy. Three slices per concentration were collected after 24 h of incubation and stored at −80 °C in 1 ml SONOP (ethanol 70 % v/v, 2 mM EDTA). The samples were homogenized with minibeadbeater (Biospec Products) for 45 s and centrifuged for 5 min at 13,200 rpm at 4 °C. The supernatant was tenfold diluted in a black 96-well plate (Costar) with Tris/EDTA buffer. The calibration curve was made using an ATP standard stock solution of 10 mg/ml (16.5 mM ATP). To every well, 50 μl luciferase (0.1 mg/ml, Roche) was added and measured after 0 and 5 min at 560 nm with Lumicount microplate luminometer (Packard).

Protein assay

To determine the amount of protein in the slices, the protein estimation by Lowry (BIO-rad DC Protein Assay) was used. The reaction involves reduction of the Folin–Coicalteau reagent (phosphotungstic phosphomolybdic acid) and oxidation of aromatic residues (mainly tryptophan, tyrosine and cysteine). The slices were completely dried overnight at 37 °C. The samples were prepared adding 200 μl of 5 M NaOH to the pellet and beads and incubated at 37 °C in the water bath while shaking. After 30 min, the samples were fivefold diluted with milliQ water and homogenized with the minibeadbeater (Biospec Products) for 40 s. To 5 μl of sample in a 96-well plate (Costar), 25 μl of Reagent A (DC™ Protein Assay, Biorad) and 200 μl of Reagent B (DC™ Protein Assay, Biorad) were added. After 15 min of incubation in the dark at room temperature, the absorbance was measured at 750 nm with Lumicount microplate luminometer (Packard).

Enzyme inhibition studies

Cytosolic rat liver thioredoxin reductase were purified according to Luthman and Holmgren [37] and mitochondrial rat liver isoform according to Rigobello et al. [73]. Thioredoxin reductases activity was determined by estimating the DTNB reduction in the presence of NADPH. Aliquots of highly purified TrxR1 (70 nM) or TrxR2 (70 nM) in 0.2 M NaKPi buffer (pH 7.4), 5 mM EDTA, and 0.25 mM NADPH were preincubated for 5 min with the various compounds, the reaction was initiated with 1 mM DTNB and followed spectrophotometrically at 412 nm for about 10 min.

Yeast glutathione reductase activity was measured in 0.2 M Tris–HCl buffer (pH 8.1), 1 mM EDTA, and 0.25 mM NADPH, after 5 min of preincubation with the various compounds. The assay was started by addition of 1 mM GSSG and followed spectrophotometrically at 340 nm.

Acknowledgments The "Centre National de la Recherche Scientifique" (ICMUB, UMR CNRS 6302) is gratefully thanked for financial support. Support was provided by the CNRS, the "Université de Bourgogne" and the "Conseil Régional de Bourgogne" through the 3MIM integrated project ("Marquage de Molécules par les Métaux pour l'Imagerie Médicale") and PARI SSTIC n°6. Dr. Fanny Picquet, Marie-José Penouilh, and Marcel Soustelle are warmly acknowledged for technical support. E. B. is thankful for COST Action TD1004 financial support. A. C. thanks the University of Groningen for funding (Rosalind Franklin Fellowship). Authors are indebted to EU COST Actions CM1105 and CM1106 for stimulating discussion. M. P. R. acknowledges PRIN 20107Z8XBW granted by the Ministero dell'Istruzione, Università e Ricerca (MIUR) (Italy), CPDA130272 granted by the University of Padova (Italy), and Consorzio Interuniversitario di Ricerca in Chimica dei Metalli nei Sistemi Biologici (CIRCSMB).

References

1. Muggia F, Farrell N (2005) Crit Rev Oncol Hematol 53:1–2
2. Barnes KR, Lippard SJ (2004) Met Ions Biol Syst 42:143–177
3. Hartinger CG, Dyson PJ (2009) Chem Soc Rev 38:391–401
4. Vessieres A, Top S, Beck W, Hillard E, Jaouen G (2006) Dalton Trans:529–541. doi:10.1039/B509984F
5. Komeda S, Casini A (2012) Curr Top Med Chem 12:219–235
6. Peacock AFA, Sadler PJ (2008) Chem Asian J 3:1890–1899
7. Claffey J, Hogan M, Müller-Bunz H, Pampillón C, Tacke M (2008) Chem Med Chem 3:729–731
8. Gasser G, Ott I, Metzler-Nolte N (2011) J Med Chem 54:3–25
9. Tiekink ER (2008) Inflammopharmacology 16:138–142
10. Nobili S, Mini E, Landini I, Gabbiani C, Casini A, Messori L (2010) Med Res Rev 30:550–580
11. Ott I (2009) Coord Chem Rev 253:1670–1681
12. Bertrand B, Casini A (2014) Dalton Trans 43:4209–4219
13. Maribel N (2009) For a review on anti-parasitic effect of gold compounds. Coord Chem Rev 253:1619–1626
14. Fiskus W, Saba N, Shen M, Ghias M, Liu J, Gupta SD, Chauhan L, Rao R, Gunewardena S, Schorno K, Austin CP, Maddocks K, Byrd J, Melnick A, Huang P, Wiestner A, Bhalla KN (2014) Cancer Res 74:2520–2532
15. See for examples of clinical trials in progress in 2014–2015. https://clinicaltrials.gov/ct2/show/NCT01747798, https://clinicaltrials.gov/ct2/show/NCT01419691, http://www.cancer.gov/clinicaltrials/search/view?cdrid=743608&version=HealthProfessional#StudyIdInfo_CD0000743608. Accessed 20 July 2015
16. Kim IS, Jin JY, Lee IH, Park SJ (2004) Brit J Pharmacol 142:749–755
17. Mirabelli CK, Johnson RK, Hill DT, Faucette LF, Girard GR, Kuo GY, Sung SM, Crooke ST (1986) J Med Chem 29:218–223
18. Scheffler H, You Y, Ott I (2010) Polyhedron 29:66–69
19. Deponte M, Urig S, Arscott LD, Fritz-Wolf K, Réau R, Herold-Mende C, Konkarevic S, Meyer M, Daviout-Charvet E, Ballou DP, Willianms CH, Becker K (2005) J Biol Chem 280:20628–20637
20. Viry E, Battaglia E, Deborde V, Müller T, Réau R, Davioud-Charvet E, Bagrel D (2008) Chem Med Chem 3:1667–1670
21. Ott I, Qian X, Xu Y, Vlecken DHW, Marques IJ, Kubutat D, Will J, Sheldrick WS, Jesse P, Prokop A, Bagowski CP (2009) J Med Chem 52:763–770
22. Bagowski CP, You Y, Scheffler H, Vlecken DH, Schmitz DJ, Ott I (2009) Dalton Trans:10799–10805
23. Ortego L, Cardoso F, Fillat MF, Laguna A, Meireles M, Villacampa MD, Gimeno MC (2014) J Inorg Biochem 130:32–37
24. Baker MV, Barnard PJ, Berners-Price SJ, Brayshaw SK, Hickley JL, Skelton BW, White AH (2006) Dalton Trans:3708–3715
25. Barnard PJ, Baker MV, Berners-Price SJ, Day AD (2004) J Inorg Biochem 98:1642–1647
26. Hickey JL, Ruhayel RA, Barnard PJ, Baker MV, Berners-Price SJ, Filipovska A (2008) J Am Chem Soc 130:12570–12571
27. Rubbiani R, Can S, Kitanovic I, Alborzinia H, Stefanopoulou M, Kokoschka M, Mönchgesang S, Sheldrick WS, Wölfl S, Ott I (2011) J Med Chem 54:8646–8657
28. Berners-Price SJ, Filipovska A (2011) Metallomics 3:863–873
29. Bindoli A, Rigobello MP, Scutari G, Gabbiani C, Casini A, Messori L (2009) Coord Chem Rev 253:1692–1707
30. Liu WK, Gust R (2013) Chem Soc Rev 42:755–773
31. Casini A, Gabbiani C, Sorrentino F, Rigobello MP, Bindoli A, Geldbach TJ, Marrone A, Re N, Hartinger CG, Dyson PJ, Messori L (2008) J Med Chem 51:6773–6781
32. Arnér ES (2009) J Biochim Biophys Acta 1790:495–526
33. Holmgren A, Lu J (2010) J Biochem Biophys Res Commun 396:120–124
34. Rhee SG, Kang SW, Chang TS, Jeong W, Kim K (2001) IUBMB Life 52:35–41
35. Huber RE, Criddle RS (1967) Arch Biochem Biophys 122:164–173
36. Citta A, Folda A, Bindoli A, Pigeon P, Top S, Vessières A, Salmain M, Jaouen G, Rigobello MP (2014) J Med Chem 57:8849–8859
37. Luthman M, Holmgren A (1982) Biochemistry 21:6628–6633
38. Rigobello MP, Callegaro MT, Barzon E, Benetti M, Bindoli A (1998) Free Radic Biol Med 24:370–376
39. Urig S, Becker K (2006) Cancer Biol 16:452–465
40. Liu Y, Li Y, Yu S, Zhao G (2012) Curr Drug Targets 13:1432–1444
41. Schuh E, Pflüger C, Citta A, Folda A, Rigobello MP, Bindoli A, Casini A, Mohr F (2012) J Med Chem 55:5518–5528
42. Citta A, Schuh E, Mohr F, Folda A, Massimino M, Bindoli A, Casini A, Rigobello MP (2013) Metallomics 5:1006–1015
43. Brigelius-Flohé R, Maiorino M (2013) Biochim Biophys Acta 1830:3289–3303
44. Lease N, Vasilevski V, Carreira M, de Almeida A, Sanaú M, Hirva P, Casini A, Contel M (2013) J. Med. Chem. 56:5806–5818
45. Pelletier F, Comte V, Massard A, Wenzel M, Toulot S, Richard P, Picquet M, Le Gendre P, Zava O, Edafe F, Casini A, Dyson PJ (2010) J Med Chem 53:6923–6933

46. Wenzel M, Bertrand B, Eymin M-J, Comte V, Harvey JA, Richard P, Groessl M, Zava O, Amrouche H, Harvey PD, Le Gendre P, Picquet M, Casini A (2011) Inorg Chem 50:9472–9480
47. Wenzel M, Bigaeva E, Richard P, Le Gendre P, Picquet M, Casini A, Bodio E (2014) J Inorg Biochem 141:10–16
48. Boseli L, Carraz M, Mazères S, Paloque L, Gonzalès G, Benoit-Vical F, Valentin A, Hemmert C, Gornitza H (2015) Organometallics 34:1046–1053
49. Lemke J, Metzler-Nolte N (2008) Eur J Inorg Chem 21:3359–3366
50. Bertrand B, Bodio E, Richard P, Picquet M, Le Gendre P, Casini A (2015) J Organomet Chem 775:124–129
51. de Graaf IAM, Olinga P, de Jager MH, Merema MT, de Kanter R, van de Kerkhof EG, Groothuis GMM (2010) Nat Protoc 5:1540–1551
52. Vickers AEM, Rose K, Fisher R, Saulnier M, Sahota P, Bentley P (2004) Toxicol Pathol 32:577–590
53. Bertrand B, Stefan L, Pirrotta M, Monchaud D, Bodio E, Richard P, Le Gendre P, Warmerdam E, de Jager MH, Groothuis GM, Picquet M, Casini A (2014) Inorg Chem 53:2296–2303
54. Daum S, Chekhun VF, Todor IN, Lukianova NY, Shvets YV, Sellner L, Putzker K, Lewis J, Zenz T, de Graaf IA, Groothuis GM, Casini A, Zozulia O, Hampel F, Mokhir A (2015) J Med Chem 58:2015–2024
55. Vergara E, Cerrada E, Clavel C, Casini A, Laguna M (2011) Dalton Trans 40:10927–10935
56. Bertrand B, de Almeida A, van der Burgt EPM, Picquet M, Citta A, Folda A, Rigobello MP, Le Gendre P, Bodio E, Casini A (2014) Eur J Inorg Chem 27:4532–4536
57. Gunatilleke SS, Barrios AM (2006) J Med Chem 49:3933–3937
58. Allen EA, Wilkinson W (1972) Spectrochim Acta Part A 28:2257–2262
59. Santini C, Pellei M, Gandin V, Porchia M, Tisato F, Marzano C (2013) Chem Rev 114:815–862
60. Srishailama A, Kumar YP, Reddya PV, Nambigari N, Vuruputuri U, Singhc SS, Satyanarayanaa S (2014) J Photochem Photobiol B Biol 132:111–123
61. Yi X, Zhao J, Sun J, Guo S, Zhang H (2013) Dalton Trans 42:2062–2074
62. Habtemariam A, Melchart M, Fernández R, Parsons S, Oswald IDH, Parkin A, Fabbiani FPA, Davidson JE, Dawson A, Aird RE, Jodrell DI, Sadler PJ (2006) J Med Chem 49:6858–6868
63. Clark RJH, Williams CS (1965) Inorg Chem 4:350–357
64. Zhanga Y, Zhaoa J, Tanga G, Zhub L (2005) Spectrochim Acta Part A 61:697–706
65. Oehninger L, Stefanopoulou M, Alborzinia H, Schur J, Ludewig S, Namikawa K, Muñoz-Castro A, Köster RW, Baumann K, Wölfl S, Sheldrick WS, Ott I (2013) Dalton Trans 42:1657–1666
66. Lu L, Zhu M (2014) Antioxid Redox Signal 20:2210–2224
67. Jungwirth U, Kowol CR, Keppler BK, Hartinger CG, Berger W, Heffeter P (2011) Antioxid Redox Signal 15:1085–1127
68. Duncan C, White AR (2012) Metallomics 4:127–138
69. van der Steen S, de Hoog P, van der Schilden K, Gamez P, Pitié M, Kiss R, Reedijk J (2010) Chem Commun 46:3568–3570
70. Uson R, Laguna A, Laguna M, Briggs DA, Murray HH, Fackler JJP (1989) Inorg Synth 26:85–91
71. Dupré N, Brazel C, Fensterbank L, Malacria M, Thorimbert S, Hasenknopf B, Lacôte E (2012) Chem Eur J 18:12962–12965
72. Busche C, Comba P, Mayboroda A, Wadepohl H (2010) Eur J Inorg Chem 2010:1295–1302
73. Rigobello MP, Bindoli A (2010) Methods Enzymol 474:109–122